

# Efficient Learning of Balanced Signed Graphs via Sparse Linear Programming

Haruki Yokota, *Student Member, IEEE*, Hiroshi Higashi, *Senior Member, IEEE*, Yuichi Tanaka, *Senior Member, IEEE*, and Gene Cheung, *Fellow, IEEE*

**Abstract**—Signed graphs are equipped with both positive and negative edge weights, encoding pairwise correlations as well as anti-correlations in data. A balanced signed graph is a signed graph with no cycles containing an odd number of negative edges. Laplacian of a balanced signed graph has eigenvectors that map via a simple linear transform to ones in a corresponding positive graph Laplacian, thus enabling reuse of spectral filtering tools designed for positive graphs. We propose an efficient method to learn a balanced signed graph Laplacian directly from data. Specifically, extending a previous linear programming (LP) based sparse inverse covariance estimation method called CLIME, we formulate a new LP problem for each Laplacian column  $i$ , where the linear constraints restrict weight signs of edges stemming from node  $i$ , so that nodes of same / different polarities are connected by positive / negative edges. Towards optimal model selection, we derive a suitable CLIME parameter  $\rho$  based on a combination of the Hannan-Quinn information criterion and a minimum feasibility criterion. We solve the LP problem efficiently by tailoring a sparse LP method based on ADMM. We theoretically prove local solution convergence of our proposed iterative algorithm. Extensive experimental results on synthetic and real-world datasets show that our balanced graph learning method outperforms competing methods and enables reuse of spectral filters, wavelets, and graph convolutional nets (GCN) constructed for positive graphs.

**Index Terms**—Signed Graph Learning, Graph Signal Processing, Sparse Linear Programming

## I. INTRODUCTION

Modern data with graph-structured kernels can be processed using mathematical tools in *graph signal processing* (GSP) such as graph transforms and wavelets [1]–[3] or deep-learning (DL)-based *graph convolutional nets* (GCN) [4]. A basic premise in graph-structured data processing is that a finite graph capturing pairwise relationships is available *a priori*; if such graph does not exist, then it must be learned from observable data—a problem called *graph learning* (GL).

A variety of GL methods exist in the literature based on statistics, signal smoothness, and diffusion kernels [5]–[7]. However, most methods focus on learning *unsigned* positive graphs, *i.e.*, graphs with positive edge weights that only encode pairwise correlations between nodes. As a consequence, most developed graph spectral filters [8]–[10] and GCNs [4] are also applicable only to positive graphs. This is understandable, as the notion of *graph spectrum* is well studied for positive graphs—*e.g.*, eigen-pairs  $(\lambda_i, \mathbf{v}_i)$  of the combinatorial graph Laplacian matrix  $\mathbf{L}$  are commonly interpreted as graph frequencies and Fourier modes, respectively [1], [3], [11]—and spectral graph filters with well-defined frequency responses

are subsequently designed for signal restoration tasks such as denoising, interpolation, and dequantization [12]–[16].

In many practical real-world scenarios, however, there exist datasets with inherent pairwise *anti-correlations*. An illustrative example is voting records in the US Senate, where Democrats / Republicans typically cast opposing votes, and thus edges between them are more appropriately modeled using *negative* weights. The resulting structure is a *signed graph*—a graph with both positive and negative edge weights [17]–[20]. However, the spectra of signed graph variation operators, such as adjacency and Laplacian matrices, are not well understood in general; for example, the nodal domain theorem [21] that shows graph Laplacian eigenvectors of increasing eigenvalues have non-decreasing number of nodal domains (*i.e.*, larger variations across kernel and hence higher frequencies) applies *only* to Laplacian matrices of positive graphs. Thus, designing spectral filters for general signed graphs remains difficult.

One exception is *balanced* signed graphs. A signed graph  $\mathcal{G}$  is balanced (denoted by  $\mathcal{G}^b$ ) if there exist no cycles with an odd number of negative edges (the formal definition is introduced in Section III-B). It is recently discovered that there exists a simple one-to-one mapping from eigenvectors  $\mathbf{U}$  of a balanced signed graph Laplacian matrix  $\mathcal{L}^b$  to eigenvectors  $\mathbf{V} = \mathbf{T}\mathbf{U}$  of a Laplacian  $\mathcal{L}^+$  for a corresponding positive graph  $\mathcal{G}^+$  (Fig. 1 Right) [22], where  $\mathbf{T}$  is a diagonal matrix with entries  $T_{i,i} \in \{1, -1\}$ . Thus, the spectrum of a balanced signed graph  $\mathcal{G}^b$  is equivalent to the spectrum of the corresponding positive graph  $\mathcal{G}^+$ , and well-studied processing tools like spectral filters for positive graphs can be readily applied to balanced signed graphs.

However, existing GL methods computing balanced signed graphs from data are limited to sub-optimal two-step approaches<sup>1</sup>: first compute a signed graph from data using, for example, *graphical lasso* (GLASSO) [24], then balance the computed signed graph via often computation-expensive balancing algorithms [25]–[27].

In this paper, we propose a computationally-efficient GL method that computes a balanced signed graph  $\mathcal{G}^b$  *directly* from observable data. Specifically, we extend a previous linear programming (LP) based sparse inverse covariance estimation method called CLIME [28] to compute a balanced signed graph Laplacian  $\mathcal{L}^b$  given a sample covariance matrix  $\mathbf{C}$ . By the *Cartwright-Harary Theorem* (CHT) [29], nodes of a balanced signed graph  $\mathcal{G}^b$  can be assigned *polarities*  $\{1, -1\}$ , so that

<sup>1</sup>The lone exception is a recent work [23], which employs a complex definition of signed graph Laplacian requiring the absolute value operator [20]. We compare against this work in performance in Section VI.

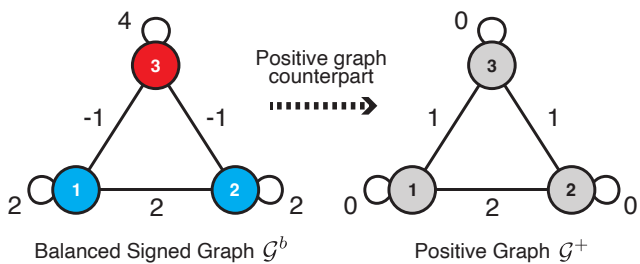


Fig. 1. Balanced signed graph (Left) and its positive graph counterpart (Right). Light-/dark-colored nodes have positive/negative polarity, respectively.

negative / positive edges connect node-pairs of different / same polarities, respectively. See Fig. 1(left) for an illustration of a balanced signed graph with nodes assigned with suitable polarities, denoted by color blue (1) and red (-1). Given CHT, the key idea is to impose additional linear sign constraints in the LP formulation on edge weights  $w_{i,j}, \forall j$ , when node  $i$  takes on an assumed polarity during optimization to maintain graph balance.

We solve the resulting *sparse linear programming* (SLP) problem for each column  $\mathbf{l}_i$  of  $\mathcal{L}^b$  representing node  $i$ 's connectivity efficiently—linear time  $\mathcal{O}(N)$  in node count  $N$  when observations  $K \ll N$ —by tailoring an *alternating direction method of multipliers* (ADMM)-based method [30]. Towards optimal model selection, for each  $\mathbf{l}_i$  we derive a suitable CLIME parameter  $\rho$  that specifies a desired sparsity level based on a combination of the Hannan-Quinn information criterion [31] and a minimum feasibility criterion. We theoretically prove local solution convergence of our proposed iterative algorithm. Experiments show that our method constructs better quality signed graph Laplacians than previous schemes [23], [26], [27], and our method enables reuse of previously designed graph filters for positive graphs [11], [32] and GCNs [4], [33] for signal denoising and interpolation.

The outline of the paper is as follows. We first overview related work in graph learning in Section II. We review basic definitions in GSP, CHT for balanced signed graphs, and sparse inverse covariance matrix learning in Section III. We formulate our balanced signed graph optimization in Section IV and present our algorithm in Section V. Experimental results and conclusion are presented in Section VI and VII, respectively.

**Notation:** Vectors and matrices are written in bold lowercase and uppercase letters, respectively. The  $(i, j)$  element of a matrix  $\mathbf{A}$  is denoted by  $A_{i,j}$ . The  $i$ -th element in the vector  $\mathbf{a}$  is denoted by  $a_i$ . The square identity matrix of rank  $N$  is denoted by  $\mathbf{I}_N$ , the  $M$ -by- $N$  zero matrix is denoted by  $\mathbf{0}_{M,N}$ , and the vector of all ones / zeros of length  $N$  is denoted by  $\mathbf{1}_N / \mathbf{0}_N$ , respectively. Operator  $\|\cdot\|_p$  denotes the  $\ell$ - $p$  norm.  $\mathbf{A} \odot \mathbf{B}$  for two matrices of the same dimension denotes the element-by-element multiplication operation.

## II. RELATED WORKS

We first divide our discussion of related works in graph learning into two subsections: i) graph learning from a statistical perspective; and ii) graph learning from a deterministic perspective. We then overview related works in spectral analysis of (balanced) signed graphs.

### A. Statistical Graph Learning

In this category, an observation matrix  $\mathbf{X} = [\mathbf{x}_1, \dots, \mathbf{x}_K] \in \mathbb{R}^{N \times K}$  composed of  $K$  signal observations is available to compute a reasonably reliable sample covariance matrix  $\mathbf{C} = \frac{1}{K-1} \mathbf{X} \mathbf{X}^\top$ . Given  $\mathbf{C}$ , GLASSO [24] estimates a sparse inverse covariance (precision) matrix, via the following formulation:

$$\min_{\Theta \succeq 0} \text{tr}(\mathbf{C}\Theta) - \log \det(\Theta) + \mu \sum_{j \neq k} |\Theta_{i,j}| \quad (1)$$

where  $\mu > 0$  is a weight parameter for the  $\ell_1$ -norm signal prior that promotes sparsity in solution  $\Theta$ . The first two terms in (1) can be interpreted as the negative log likelihood.

Extensions of GLASSO abound: [34] constrained solutions  $\Theta$  to be sets of targeted categories of graph Laplacian matrices (*e.g.*, combinatorial Laplacians); [35] constrained the patterns of the Laplacian eigenvalues so that the obtained graph has desirable properties; [36] restricted solutions  $\Theta$  to contain a pre-chosen set of core eigenvectors. While we also pursue a statistical approach, instead of GLASSO, we start from the linear programming (LP) based CLIME formulation [28], which is more amenable to new constraints that dictate balanced signed graph Laplacian matrices, as we show in Section IV.

### B. Deterministic Graph Learning

In scenarios where sufficient signal observations are not available to obtain a reliable sample covariance  $\mathbf{C}$ , a graph can still be estimated based on additional assumptions. One popular assumption is that the limited observed signals are all smooth w.r.t. the underlying graph [6], [37], [38]. For example, [37] employed the *graph Laplacian regularizer* (GLR) [9],  $\text{tr}(\mathbf{X}^\top \mathbf{L} \mathbf{X})$ —a signal smoothness measure for  $\mathbf{X}$  given graph specified by  $\mathbf{L}$ —to regularize an ill-posed problem when seeking Laplacian  $\mathbf{L}$ . However, the assumption on individual signal smoothness may be too strong for some scenarios.

Another popular assumption is the diffusion model [7]: in a time series of signals  $\mathcal{X} = \{\mathbf{x}_0, \mathbf{x}_1, \dots\}$ , the signals evolve following differential equation  $\frac{\partial \mathbf{x}}{\partial t} = \tau \mathbf{L} \mathbf{x}$ , resulting in solution  $\mathbf{x}(t) = e^{-\tau t \mathbf{L}} \mathbf{x}_0$ , where  $\mathbf{x}_0$  is the initial signal at time  $t = 0$ . [7] proposed an efficient algorithm to compute  $\mathbf{L}$  given  $\mathcal{X}$  with an additional sparsity assumption. Clearly, diffusion models do not apply in scenarios where observed data  $\mathcal{X}$  are not evolving signals over time. Further, even for data in a time series, it is not clear that the pairwise relationships would remain static, resulting in a single fixed graph structure [39].

Finally, there exist graph learning methods where the assumption is that relevant feature vector  $\mathbf{f}_i$  can be computed for each node  $i$ , so that edge weights of a similarity graph can be computed as function of feature distances [40], [41]. Specifically, weight  $w_{i,j}$  of edge  $(i, j)$  can be computed as

$$w_{i,j} = \exp(-d_{i,j}) \\ d_{i,j} = (\mathbf{f}_i - \mathbf{f}_j)^\top \mathbf{M} (\mathbf{f}_i - \mathbf{f}_j) \quad (2)$$

where  $d_{i,j}$  is the squared feature (Mahalanobis) distance,  $\mathbf{f}_i \in \mathbb{R}^K$  is a  $K$ -dimensional feature vector, and  $\mathbf{M} \succeq 0$  is a *positive semi-definite* (PSD) *metric matrix*. Feature vectors  $\mathbf{f}_i$  can be either hand-crafted or learned directly from data [42], and the optimization of  $\mathbf{M}$  is called *metric learning* [41].

*Bilateral filter* (BF) [43] in image denoising is an example of (2), where  $\mathbf{f}_i$  contains a pixel's intensity and 2D grid location, and  $\mathbf{M}$  is a diagonal matrix  $\mathbf{M} = \text{diag}(1/\sigma_d^2, 1/\sigma_r^2)$ . One possible direction is to consider both signal statistics in sample covariance  $\mathbf{C}$  and features  $\{\mathbf{f}_i\}$  when estimating an appropriate similarity graph; we leave this exploration for future work.

### C. Spectral Analysis of Signed Graphs

While most spectral analysis works in GSP are done on positive graphs with non-negative edge weights [1]–[3], there are recent efforts studying graph frequencies on signed graphs. Seminally, [44] defined a signed graph Laplacian  $\mathbf{L}^s \triangleq \mathbf{D}^s - \mathbf{W}$  for a signed graph, where the degree  $D_{i,i}^s$  of a node  $i$  is the sum of the absolute value weights  $|w_{i,j}|$  of edges  $(i, j)$  stemming from  $i$ . This ensures a PSD Laplacian  $\mathbf{L}^s$  and non-negative eigenvalues interpretable as graph frequencies. Using this definition, [23] proposed new methods to learn a signed graph Laplacian from data. However, when given a sample covariance matrix  $\mathbf{C}$  computed from observed data, how to learn a (sparse) Laplacian  $\mathbf{L}^s$  that best reflects statistics in  $\mathbf{C}$  is not straightforward, given the nonlinear absolute value operator. In our experiments, we demonstrate better performance of our method over [23] in different graph learning settings.

Spectral properties of balanced signed graphs were studied in [41], where it was proven that the left-ends of Gershgorin discs of a balanced signed graph Laplacian  $\mathcal{L}^b$  can be perfectly aligned at its minimum eigenvalue  $\lambda_{\min}(\mathcal{L}^b)$  via a similarity transform derived from its first eigenvector  $\mathbf{v}_1$ . [22] proved that there exists a one-to-one mapping of eigenvectors of a balanced graph Laplacian matrix  $\mathcal{L}^b$  to eigenvectors of a positive graph Laplacian  $\mathcal{L}^+$  via a similarity transform derived from node polarities. Thus, graph frequencies of a balanced signed graph  $\mathcal{G}^b$  are exactly those of the corresponding positive graph  $\mathcal{G}^+$ , which is well understood in the GSP literature by way of the nodal domain theorem [21]. [22] motivates this work; learning a balanced signed graph Laplacian  $\mathcal{L}^b$  from sample covariance  $\mathbf{C}$  enables us to reuse spectral filters designed for positive graphs  $\mathcal{G}^+$  to process signals on balanced signed graphs  $\mathcal{G}^b$ .

**Improvements from Conference Version:** This paper extends from our conference version [45] in the following ways:

- 1) Instead of an off-the-shelf LP solver with complexity  $\mathcal{O}(N^{2.055})$  [46], we solve each SLP problem for a column  $\mathbf{l}_i$  in balanced graph Laplacian  $\mathcal{L}^b$  via a novel adaptation of ADMM [30], resulting in linear-time complexity  $\mathcal{O}(N)$  when  $K \ll N$ ;
- 2) We derive the important CLIME parameter  $\rho$  that specifies a desired sparsity level based on Hannan-Quinn information criterion [31] and a minimum feasibility criterion, leading to overall performance improvement;
- 3) We theoretically prove convergence of our iterative algorithm to a local minimum solution; and
- 4) We conducted extensive experiments on synthetic data and four real-world datasets with non-negligible anti-correlations, showing superiority of our algorithm.

### III. PRELIMINARIES

We first formally define signed graphs and balanced signed graphs. We then review a sparse inverse covariance matrix

TABLE I  
NOTATIONS USED IN ALGORITHM DEVELOPMENT

Notations	Descriptions
$\mathcal{G}(\mathcal{V}, \mathcal{E}, \mathbf{W})$	Graph with nodes $\mathcal{V}$ , edges $\mathcal{E}$ , adjacency matrix $\mathbf{W}$
$\mathcal{G}^b$	Balanced signed graph
$\mathcal{L}^b \in \mathbb{R}^{N \times N}$	Laplacian matrix for balanced signed graph
$\mathcal{G}^+$	Positive graph
$\mathcal{L}^+ \in \mathbb{R}^{N \times N}$	Laplacian matrix for positive graph
$\mathbf{X} \in \mathbb{R}^{N \times K}$	Observation matrix
$\mathbf{C} \in \mathbb{R}^{N \times N}$	sample covariance matrix
$\mathbf{l}_i \in \mathbb{R}^N$	$i$ -th column of balanced signed graph Laplacian $\mathcal{L}^b$
$\mathbf{e}_i \in \mathbb{R}^N$	$i$ -th canonical vector
$\rho \in \mathbb{R}_+$	CLIME parameter specifying sparsity level
$\beta_i \in \{-1, 1\}$	Polarity of node $i$
$\mathbf{S}^i \in \mathbb{R}^{N \times N}$	Diagonal matrix with entries $S_{j,j}^i = \beta_i \beta_j$
$\bar{\mathbf{I}} \in \mathbb{R}^N$	Upper-bound variable $\bar{\mathbf{I}} \geq \pm \mathbf{l}_i$
$\mathbf{r} \in \mathbb{R}^N$	Dependent variable $\mathbf{r} \triangleq \mathbf{C} \mathbf{l}_i - \mathbf{e}_i$
$\mathbf{q} \in \mathbb{R}^{5N}$	Non-negative slack variable
$\mathbf{x} \in \mathbb{R}^{3N}$	Main variable $\mathbf{x} = [\bar{\mathbf{I}}; \mathbf{l}_i; \mathbf{r}]$ in (20)
$\mathbf{c} \in \mathbb{R}^{3N}$	Cost vector $\mathbf{c} \triangleq [\mathbf{1}_N; \mathbf{0}_{2N}]$ in (20)
$\tilde{\mathbf{q}} \in \mathbb{R}^{5N}$	Auxiliary variable
$\boldsymbol{\mu} \in \mathbb{R}^{11N}$	Lagrange multiplier
$\gamma \in \mathbb{R}_+$	ADMM parameter

estimation algorithm called CLIME [28]. See Table I for a list of notations.

#### A. Signed Graphs

Denote by  $\mathcal{G}(\mathcal{V}, \mathcal{E}, \mathbf{W})$  an undirected signed graph with node set  $\mathcal{V} = \{1, \dots, N\}$ , edge set  $\mathcal{E}$ , and symmetric weighted adjacency matrix  $\mathbf{W} \in \mathbb{R}^{N \times N}$ , where weight of edge  $(i, j) \in \mathcal{E}$  connecting nodes  $i, j \in \mathcal{V}$  is  $w_{i,j} = W_{i,j} \in \mathbb{R}$ . We assume that  $W_{i,j}, \forall i \neq j$ , can be positive / negative to encode pairwise correlation / anti-correlation, while (possible) self-loop weight  $w_{i,i}$  is non-negative, i.e.,  $W_{i,i} \geq 0, \forall i$ . Denote by  $\mathbf{D} \in \mathbb{R}^{N \times N}$  a diagonal *degree matrix*, where  $D_{i,i} = \sum_j W_{i,j}$ . We define the symmetric *generalized graph Laplacian matrix*<sup>2</sup> for  $\mathcal{G}$  as  $\mathcal{L} \triangleq \mathbf{D} - \mathbf{W} + \text{diag}(\mathbf{W})$  [2].

#### B. Balanced Signed Graphs

A signed graph is balanced if there are no cycles with an odd number of negative edges—the product of edge weights in any cycle is positive [29]. We rephrase an equivalent definition of balanced signed graphs, known as *Cartwright-Harary Theorem* (CHT), as follows.

**Theorem 1.** *A signed graph  $\mathcal{G}(\mathcal{V}, \mathcal{E}, \mathbf{W})$  is balanced if and only if each node  $i \in \mathcal{V}$  can be assigned polarity  $\beta_i \in \{1, -1\}$ , such that a positive / negative edge always connects nodes of the same / opposite polarities, i.e.  $\beta_i \beta_j = \text{sign}(W_{i,j})$ .*

In other words, a signed graph is balanced if all graph nodes can be partitioned into two disjoint sets  $\mathcal{V}_1$  and  $\mathcal{V}_{-1}$ , such that all edges *within* a set  $\mathcal{V}_k, k \in \{1, -1\}$ , are positive, and all edges *between* the two sets  $\mathcal{V}_1$  and  $\mathcal{V}_{-1}$  are negative. In this case, the edges are said to be *consistent*. In [22], the notion of consistent edges in a balanced graph is defined as follows:

<sup>2</sup>We use the generalized graph Laplacian for signed graphs instead of the signed graph Laplacian definition in [20] that requires the absolute value operator. This leads to a simple mapping of eigenvectors of our signed graph Laplacian to ones of a corresponding positive graph Laplacian, and a straightforward LP problem formulation extending from [28].

**Definition 1.** A consistent edge  $(i, j) \in \mathcal{E}$  with weight  $W_{i,j}$  is a positive / negative edge connecting two nodes of the same / opposite polarities, i.e.,  $\beta_i \beta_j = \text{sign}(W_{i,j})$ .

### C. Mapping to Positive Graph Counterpart

We define the Laplacian  $\mathcal{L}^+$  for the positive graph counterpart  $\mathcal{G}^+$  of a balanced signed graph  $\mathcal{G}^b$  as  $\mathcal{L}^+ \triangleq \mathbf{D} - |\mathbf{W}| + \text{diag}(\mathbf{W})$ , where  $|\mathbf{W}|$  denotes a matrix with element-wise absolute value of  $\mathbf{W}$ . A positive graph  $\mathcal{G}^+$  has its own adjacency matrix<sup>3</sup>  $\mathbf{W}^+$ , where  $W_{i,j}^+ = |W_{i,j}|, \forall i \neq j$ , and  $W_{i,i}^+ = W_{i,i} - 2 \sum_j [-W_{i,j}]_+$ , where  $[c]_+$  is a positivity function that returns  $c$  if  $c \geq 0$  and 0 otherwise. The diagonal degree matrix  $\mathbf{D}^+$  for  $\mathcal{G}^+$  is defined conventionally, where  $D_{i,i}^+ = \sum_j W_{i,j}^+$ . Note that the adjacency matrix  $\mathbf{W}^+$  is so defined such that

$$\mathcal{L}^+ = \mathbf{D} - |\mathbf{W}| + \text{diag}(\mathbf{W}) = \mathbf{D}^+ - \mathbf{W}^+ + \text{diag}(\mathbf{W}^+). \quad (3)$$

One can show via the *Gershgorin circle theorem* (GCT) [48] that a sufficient condition for any  $\mathcal{L}^+$  to be *positive semi-definite* (PSD) is  $\text{diag}(\mathbf{W}^+) \geq \mathbf{0}_N$ . For illustration, in Fig. 1, we show an example of a balanced signed graph  $\mathcal{G}^b$  and its positive graph counterpart  $\mathcal{G}^+$ .

A balanced signed graph Laplacian  $\mathcal{L}^b = \mathbf{U}\mathbf{A}\mathbf{U}^\top$  of  $\mathcal{G}^b$  enjoys a one-to-one mapping of its eigenvectors to those of its positive graph counterpart  $\mathcal{L}^+$  [22]. Specifically, suppose we partition the nodes of a balanced signed graph  $\mathcal{G}^b = (\mathcal{V}, \mathcal{E})$ , into two disjoint sets  $\mathcal{V}_1$  and  $\mathcal{V}_{-1}$  and we reorder rows / columns of balanced signed graph Laplacian  $\mathcal{L}^b$ , so that nodes in  $\mathcal{V}_1$  of size  $M$  are indexed before nodes in  $\mathcal{V}_{-1}$  of size  $N - M$ . Then, using the following invertible diagonal matrix

$$\mathbf{T} = \begin{bmatrix} \mathbf{I}_M & \mathbf{0}_{M,N-M} \\ \mathbf{0}_{N-M,M} & -\mathbf{I}_{N-M} \end{bmatrix}, \quad (4)$$

we can show that  $\mathcal{L}^b$  and  $\mathcal{L}^+$  are *similarity transform* of each other:

$$\begin{aligned} \mathbf{T}\mathcal{L}^b\mathbf{T}^{-1} &\stackrel{(a)}{=} \mathbf{T}\mathbf{U}\mathbf{A}\mathbf{U}^\top\mathbf{T}^\top \stackrel{(b)}{=} \mathbf{V}\mathbf{A}\mathbf{V}^\top \\ &\stackrel{(c)}{=} \mathbf{T}(\mathbf{D} - \mathbf{W} + \text{diag}(\mathbf{W}))\mathbf{T} \\ &= \mathbf{D} - |\mathbf{W}| + \text{diag}(\mathbf{W}) = \mathcal{L}^+ \end{aligned} \quad (5)$$

where in (a) we write  $\mathbf{T}^\top = \mathbf{T}^{-1} = \mathbf{T}$ , in (b)  $\mathbf{V} \triangleq \mathbf{T}\mathbf{U}$ , and in (c) we apply the definition of generalized graph Laplacian. Thus,  $\mathcal{L}^+$  and  $\mathcal{L}^b$  have the same set of eigenvalues, and their eigen-matrices are related via matrix  $\mathbf{T}$ . For the example in Fig. 1, since the signed graph on the left is balanced,  $\mathcal{L}^+$  is a similar transform of  $\mathcal{L}^b$  via diagonal matrix  $\mathbf{T} = \text{diag}([1, 1, -1])$ .

### D. Spectral Graph Filters

Spectral graph filters are frequency modulating filters, where graph frequencies are conventionally defined as the *non-negative* eigenvalues of a PSD graph Laplacian [2]. Thus, to reuse spectral filters designed for positive graphs in the

<sup>3</sup>The use of a self-loop of weight equaling to twice the sum of connected negative edge weights is also done in [47].

literature [10] for a balanced signed graph  $\mathcal{G}^b$ , it is sufficient to require  $\text{diag}(\mathbf{W}^+) \geq \mathbf{0}$  for the adjacency matrix  $\mathbf{W}^+$  of the positive graph counterpart  $\mathcal{G}^+$  [49]. This condition translates to self-loops of weights  $W_{i,i} \geq 2 \sum_j [-W_{i,j}]_+, \forall i$ , for the balanced signed graph  $\mathcal{G}^b$ .

### E. Sparse Inverse Covariance Learning

Given a data matrix  $\mathbf{X} = [\mathbf{x}_1, \dots, \mathbf{x}_K] \in \mathbb{R}^{N \times K}$  where  $\mathbf{x}_k \in \mathbb{R}^N$  is the  $k$ th signal observation, a sparse inverse covariance matrix  $\mathcal{L} \in \mathbb{R}^{N \times N}$  (interpretable as a signed graph Laplacian) can be estimated from data via a constrained  $\ell_1$ -minimization formulation called CLIME [28]. In a nutshell, CLIME seeks  $\mathcal{L}$  given a sample covariance matrix<sup>4</sup>  $\mathbf{C} = \frac{1}{K-1}\mathbf{X}\mathbf{X}^\top$  (assuming zero mean) via a *linear programming* (LP) formulation:

$$\min_{\mathcal{L}} \|\mathcal{L}\|_1, \quad \text{s.t.} \quad \|\mathbf{C}\mathcal{L} - \mathbf{I}_N\|_\infty \leq \rho \quad (6)$$

where  $\rho \in \mathbb{R}_+$  is a positive scalar parameter. Specifically, (6) computes a sparse  $\mathcal{L}$  (promoted by the  $\ell_1$ -norm objective) that approximates the right inverse of  $\mathbf{C}$ . The  $i$ th column  $\mathbf{l}_i$  of  $\mathcal{L}$  can be computed independently:

$$\min_{\mathbf{l}_i} \|\mathbf{l}_i\|_1, \quad \text{s.t.} \quad \|\mathbf{C}\mathbf{l}_i - \mathbf{e}_i\|_\infty \leq \rho \quad (7)$$

where  $\mathbf{e}_i$  is the canonical vector with one at the  $i$ -th entry and zero elsewhere. (7) can be solved using an off-the-shelf LP solver such as [46] with complexity  $\mathcal{O}(N^{2.055})$ . The resulting  $\mathcal{L} = [\mathbf{l}_1, \mathbf{l}_2, \dots, \mathbf{l}_N]$  is not symmetric in general, and [28] computes a symmetric approximation  $\mathcal{L}^* \triangleq (\mathcal{L} + \mathcal{L}^\top)/2$  as a post-processing step. In [50], CLIME is extended to learn a complex-valued Hermitian graph Laplacian matrix.

## IV. BASELINE BALANCED SIGNED GRAPH OPTIMIZATION

We first overview our optimization approach to learn a generalized Laplacian  $\mathcal{L}^b$  corresponding to a balanced signed graph  $\mathcal{G}^b$ , given a sample covariance matrix  $\mathbf{C}$ . We then formulate an LP-based optimization for each column  $\mathbf{l}_i$  of  $\mathcal{L}^b$ , extended from CLIME [28]. An overview of the proposed method is shown in Fig. 2.

### A. Optimization Approach

Our goal is to estimate a balanced signed graph Laplacian  $\mathcal{L}^b \in \mathbb{R}^{N \times N}$  directly from  $\mathbf{C} = \frac{1}{K-1}\mathbf{X}\mathbf{X}^\top$ . In essence, our algorithm optimizes polarity  $\beta_i \in \{-1, 1\}$  and edge weights  $w_{i,j}$ 's stemming from one node  $i \in \{1, \dots, N\}$  at a time, and terminates when the objective no longer improves. As discussed in Section III-B, CHT states that in a balanced signed graph, same- / opposite-polarity node pairs can only be connected by edges of positive / negative weights, respectively. Given the edge sign restrictions of a balanced graph dictated by CHT, for each node  $i$ , we execute a variant of optimization (7) *twice*—one for each possible polarity  $\beta_i$ —where the signs of the entries in variable  $\mathbf{l}_i$  (weight of edges stemming from node  $i$ ) are restricted for consistency. We then adopt node  $i$ 's

<sup>4</sup>sample covariance matrix  $\mathbf{C}$  is *positive definite* (PD) if  $K \geq N$ . We consider both cases,  $K \geq N$  and  $K \ll N$ , in the sequel.

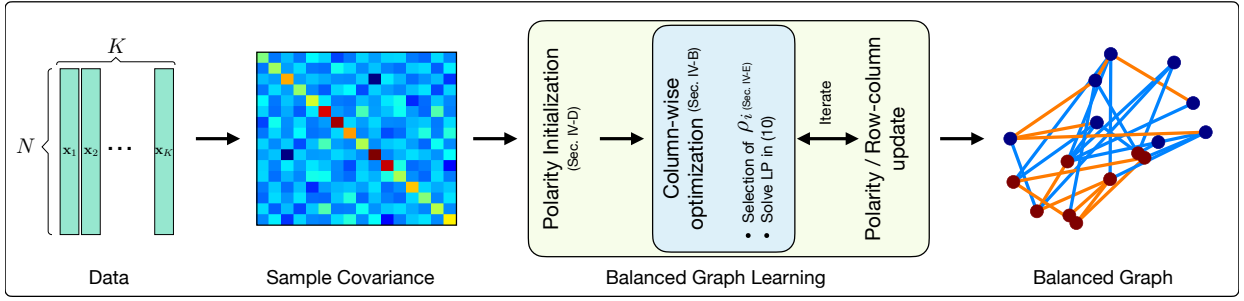


Fig. 2. Overview of proposed balanced graph learning approach.

polarity  $\beta_i$  corresponding to the smaller of the two objective values as the optimal polarity.

Specifically, our optimization procedure is as follows:

- 1) Initialize polarities  $\beta_j$  for all graph nodes  $j$ .
- 2) For each column  $\mathbf{l}_i$  of  $\mathcal{L}^b$  corresponding to node  $i$ ,
  - a) Assume node  $i$ 's polarity  $\beta_i \in \{1, -1\}$ .
  - b) Optimize  $\mathbf{l}_i$  while restricting  $\text{sign}(l_{i,j})$  so that  $l_{i,j}$ 's are consistent with polarities of connected nodes  $j$ .
  - c) Smaller of the two objective values corresponding to assumptions  $\beta_i = 1$  and  $\beta_i = -1$  determines node  $i$ 's polarity.
  - d) Update  $i$ th column/row of  $\mathcal{L}^b$  using computed  $\mathbf{l}_i$ .
- 3) Continue updating columns of  $\mathcal{L}^b$  until convergence.

Note that by simultaneously updating the  $i$ th column / row of  $\mathcal{L}^b$  in step 2(d),  $\mathcal{L}^b$  remains symmetric.

An alternative approach is to alternately optimize edge weight magnitudes in  $\mathcal{L}^b$  and the node-polarity matrix  $\mathbf{B} = \beta\beta^\top$  for  $\beta = [\beta_1, \dots, \beta_N]$ , where the optimization of  $\mathbf{B}$  is formulated as a *semi-definite programming* (SDP) problem [51]. However, computation of a general SDP is expensive (at least  $\mathcal{O}(N^3)$ ). Further, the initial polarities extracted from the covariance matrix (described in Section IV-D) have proven sufficiently accurate, and thus few further updates are necessary.

### B. Linear Constraints for Consistent Edges

To reformulate CLIME for a balanced signed graph Laplacian  $\mathcal{L}^b$ , we first construct linear constraints that ensure consistent edges. From Definition 1, we rewrite the edge consistency restriction  $\beta_i\beta_j = \text{sign}(W_{i,j})$  for an edge  $(i, j) \in \mathcal{E}$  of the target balanced graph  $\mathcal{G}^b$ , given node polarities  $\beta_i$  and  $\beta_j$ , as

$$\beta_i\beta_j \text{sign}(W_{i,j}) = \begin{cases} 1 & \text{if } (i, j) \text{ is consistent} \\ -1 & \text{if } (i, j) \text{ is inconsistent} \end{cases}. \quad (8)$$

For each Laplacian entry  $\mathcal{L}_{i,j}^b$ , linear constraint for edge consistency, given node polarities  $\beta_i$  and  $\beta_j$ , is thus

$$\beta_i\beta_j\mathcal{L}_{i,j}^b \leq 0, \quad \forall j | j \neq i. \quad (9)$$

### C. Optimization of Laplacian Column

We can now reformulate the LP problem (7) by incorporating linear constraints (9). Denote by  $\mathbf{S}^i \in \mathbb{R}^{N \times N}$  a diagonal matrix for optimization of  $\mathbf{l}_i$ , where each diagonal entry is  $S_{j,j}^i = \beta_i\beta_j$ . Optimization (7) becomes

$$\min_{\mathbf{l}_i} \|\mathbf{l}_i\|_1 \quad \text{s.t.} \quad \begin{cases} \|\mathbf{C}\mathbf{l}_i - \mathbf{e}_i\|_\infty \leq \rho_i \\ \mathbf{S}^i\mathbf{l}_i \leq \mathbf{0}_N \end{cases}. \quad (10)$$

The vector inequality here represents entry-wise inequality. By incorporating one more linear constraint, (10) remains an LP. Note that the original formulation (7) assumes a single parameter  $\rho$  for all columns. However, there is no guarantee that each column enjoys the same sparsity. So in our formulation, we adaptively set  $\rho_i$  for each column-wise LP.

1) *Feasibility of (10)*: Unlike (7) that always has at least one feasible solution for any  $\rho > 0$  (*i.e.*,  $i$ th column of  $\mathbf{C}^{-1}$ , assuming  $K \geq N$ ), the additional inequality constraint in (10) means that the LP may be *infeasible*. Thus, the selection of  $\rho_i$  is particularly crucial for (10); we discuss this issue in Section IV-E. Assuming that the LP (10) is feasible for every  $i$ , we prove local convergence of our iterative algorithm for  $\mathcal{L}^b$  in Section IV-F. Instead of using an off-the-shelf solver like [46] designed for general LP, we tailor an ADMM-based method [30] for our particular LP (10) in Section V, which has a speed advantage for the  $K \ll N$  case.

2) *Mismatch of Statistical Models*: In general, the statistics (inverse covariance  $\mathbf{C}^{-1}$ ) of a given dataset may not be a balanced signed graph Laplacian. Thus, by proactively enforcing graph balance in (10), the computed Laplacian  $\mathcal{L}^b$  may suffer from mismatch to the true statistics of the data. However, there are empirical evidence that many datasets in practice do tend towards graph balance, including social, biological, economic, and collaborative networks [52]–[55]. For example, two people  $A$  and  $B$  having a mutual friend  $C$  are likely to be friends themselves, resulting in a balanced triad  $(A, B, C)$ . In our experiments in Section VI, we demonstrate that for many real-world datasets, the benefits of learning a balanced signed graph (*e.g.*, enabling positive graph spectral filtering) outweigh the cost of potential statistical mismatches.

### D. Initial Nodal Polarity Assignments

As discussed in Section IV-A, initialization of node polarities  $\{\beta_i\}$  is an important first step. We describe a simple strategy given sample covariance  $\mathbf{C} = \frac{1}{K-1}\mathbf{X}\mathbf{X}^\top$ . By definition, sample covariance  $C_{i,j}$  between nodes  $i$  and  $j$  is computed as (assuming zero mean)

$$C_{i,j} = \frac{1}{K-1} \sum_{k=1}^K X_{i,k}X_{j,k}. \quad (11)$$

We compute the *variance of covariance*<sup>5</sup> (VoC),  $V_{i,j}$  of  $C_{i,j}$ —*i.e.*, how much each component  $X_{i,k}X_{j,k}$  deviates from  $C_{i,j}$ —as

$$V_{i,j} = \frac{1}{K-1} \sum_{k=1}^K (X_{i,k}X_{j,k} - C_{i,j})^2. \quad (12)$$

Given that the sample variance is not robust statistics (and thus sensitive to outliers) [56], a small VoC  $V_{i,j}$  would indicate that the estimated  $C_{i,j}$  is more reliable.

Hence, we compute a weight  $u_{i,j}$  for each entry  $(i,j)$  in matrix  $\mathbf{C}'$  using an exponential kernel:

$$u_{i,j} = \exp\left(-\frac{V_{i,j}}{\sigma_v^2}\right) \quad (13)$$

where  $\sigma_v > 0$  is a parameter. Given that VoC  $V_{i,j} \geq 0$ , weight  $u_{i,j} \in (0, 1]$ . Using this weighted covariance matrix  $\mathbf{C}' = \mathbf{U} \odot \mathbf{C}$ , we can initialize node polarities as follows.

First, find the entry  $(i,j)$  in  $\mathbf{C}'$  with the largest magnitude  $|C'_{i,j}|$ . If  $|C'_{i,j}| > 0$ , then assign 1 to both  $\beta_i$  and  $\beta_j$ ; otherwise, assign  $\beta_i \leftarrow 1$  and  $\beta_j \leftarrow -1$ . Next, initialize *polarity set*  $\mathcal{P} = \{i, j\}$ . Start from the empty set. Find a neighbor  $k \in \mathcal{N} \setminus \mathcal{P}$  connected to a node  $p \in \mathcal{P}$  with the largest magnitude  $|C'_{k,p}|$ . Assign  $\beta_k \leftarrow \text{sign}(C'_{k,p})\beta_p$ . Add  $k$  to set  $\mathcal{P}$ . Repeat till all nodes are assigned polarities. This procedure maximally preserves the signs of entries in  $\mathbf{C}'$  during polarity assignments.

#### E. Choosing CLIME Parameter $\rho_i$

There are two considerations when choosing parameter  $\rho_i$  in (10): i) *statistically*, what is the best *model selection* [57]–[59]—specified by  $\rho^\circ$ —given the numbers of model parameters and observations in (10)? ii) *deterministically*, what is the minimum  $\rho^l$  so that LP (10) is feasible?  $\rho^\circ$  is a generally good value trading off the model complexity with model fit given our problem setup.  $\rho^l$  is a lower bound value at which the specific LP (10) is guaranteed feasible. We discuss these two considerations next.

1) **Hannan-Quinn Information Criterion:** An information criterion balances between goodness of fit with model complexity. We choose to minimize the *Hannan-Quinn information criterion* (HQIC) [31] for (10), defined as

$$\text{HQIC} = -2L_{\max} + 2k \ln(\ln(K)) \quad (14)$$

where  $L_{\max}$  is the log likelihood,  $k$  is the number of parameters, and  $K$  is the number of observations. Compared to *Akaike Information Criterion* (AIC) [57] and *Baysian Information Criterion* (BIC) [58], HQIC is known for its strong consistency; *i.e.*, as the sample size increases, HQIC is more likely to select the true model. For our specific problem setup in (10), we can compute HQIC for an estimated graph Laplacian  $\mathcal{L}$  as

$$\text{HQIC}(\rho) = -2(\log \det(\mathcal{L}) - \text{tr}(\mathbf{C}\mathcal{L})) + 2k \ln(\ln(K)), \quad (15)$$

where  $k$  is the number of non-zero elements in the upper triangular part of  $\mathcal{L}$ . Optimal  $\rho^\circ$  can be searched via the following steps: 1) Estimate  $\mathcal{L}$  with a candidate parameter  $\rho^c$ ; 2) compute HQIC( $\rho^c$ ) given estimated  $\mathcal{L}$ ; and 3) increment  $\rho^c$  by a small  $\delta$  towards a local minimum HQIC( $\rho^c$ ).

<sup>5</sup>It can be shown that the variance of the variance can be expressed as the second and the fourth moments of a random variable.

2) **Choosing  $\rho_i$  for Minimum Feasibility:** For the first time LP (10) is executed for a particular node  $i$ , we compute  $\rho^l$  to ensure (10) has at least a feasible solution  $\mathbf{l}_i$ . To accomplish this, we compute the following LP for variables  $\mathbf{l}_i$  and  $\rho$ :

$$\min_{\mathbf{l}_i, \rho} \rho, \quad \text{s.t.} \quad \begin{cases} \mathbf{e}_i - \rho \mathbf{1} \leq \mathbf{C}\mathbf{l}_i \leq \mathbf{e}_i + \rho \mathbf{1} \\ \mathbf{S}^i \mathbf{l}_i \leq \mathbf{0}_N \\ \rho \geq 0 \end{cases}. \quad (16)$$

(16) computes the smallest  $\rho \geq 0$  so that at least one feasible solution  $\mathbf{l}_i$  satisfies the linear constraints in (10). The solution to (16) is  $\rho^l$ .

3) **Choosing  $\rho_i$  for Previous Solution Feasibility:** In subsequent iterations when a previous solution  $\mathbf{l}_i^l$  is available to (10), to ensure algorithm convergence (see Section IV-F) we compute  $\rho^l$  to ensure  $\mathbf{l}_i^l$  remains feasible. To accomplish this, we compute the following LP for  $\rho \geq 0$ :

$$\min_{\rho} \rho, \quad \text{s.t.} \quad \begin{cases} \mathbf{e}_i - \rho \mathbf{1} \leq \mathbf{C}\mathbf{l}_i^l \leq \mathbf{e}_i + \rho \mathbf{1} \\ \rho \geq 0 \end{cases} \quad (17)$$

assuming  $\mathbf{S}^i \mathbf{l}_i^l \leq \mathbf{0}_N$ . Using the solution  $\rho^l$  to (17) to compute (10) ensures that previous solution  $\mathbf{l}_i^l$  remains feasible.

The graph estimated using  $\rho^l$  tends to be dense and has high HQIC. Thus, we initialize  $\rho_i \leftarrow \rho^l$ , then increment  $\rho_i$  by  $\delta$  (thus ensuring solution feasibility) until an optimal  $\rho^\circ$  that gives the smallest HQIC.

#### F. Algorithm Convergence

Given our  $\rho_i$  selection, we prove that our iterative algorithm converges to a local minimum. We note first that given the overall objective  $\|\mathcal{L}\|_1 = \sum_i \|\mathbf{l}_i\|_1$  is lower-bounded by zero, it is sufficient to prove solution convergence by showing that objective  $\|\mathcal{L}\|_1$  is *monotonically non-increasing* as the algorithm iterates.

At the start of an iteration optimizing  $\mathbf{l}_i$ , the  $i$ th column / row of  $\mathcal{L}$  has just been updated to  $\mathbf{l}_i^l$  during previous iteration optimizing  $\mathbf{l}_{i-1}$ ; *i.e.*, the  $(i-1)$ -th entry of  $\mathbf{l}_i$  have been updated. For the current iteration, we choose  $\rho$  large enough that  $\mathbf{l}_i^l$  remains in the feasible solution space (via LP (17)). With this choice, the optimal solution  $\mathbf{l}_i^*$  obtained at iteration  $t$  with the same polarity satisfies

$$\|\mathbf{l}_i^*\|_1 \leq \|\mathbf{l}_i^l\|_1. \quad (18)$$

Node  $i$  switches polarity only if the objective value obtained with opposite polarity is strictly smaller than  $\|\mathbf{l}_i^*\|_1$ . Hence, whether the polarity changes or not,  $\|\mathcal{L}\|_1$  is monotonically non-increasing.

### V. FAST BALANCED SIGNED GRAPH OPTIMIZATION

#### A. LP in Standard Form

Towards efficient computation, we treat (10) as a *sparse linear programming* (SLP) problem<sup>6</sup>, efficiently solvable via a novel adaptation of ADMM that split variables for alternating optimizations until solution convergence [30].

<sup>6</sup>By SLP, we mean that the coefficient matrix  $\mathbf{A}$  in the linear constraint  $\mathbf{A}\mathbf{x} = \mathbf{b}$  in an LP standard formulation is sparse.

We first rewrite (10) into LP standard form. First, define *upper-bound variable*  $\tilde{\mathbf{l}} \in \mathbb{R}^N$ , with additional linear constraints  $\tilde{\mathbf{l}} \geq \pm \mathbf{l}_i$ . This enables a linear objective  $\mathbf{1}_N^\top \tilde{\mathbf{l}}$  for a minimization problem (thus ensuring the upper bound is tight, *i.e.*,  $\tilde{\mathbf{l}} = |\mathbf{l}_i|$ ). Define also *dependent variable*  $\mathbf{r} \triangleq \mathbf{C}\mathbf{l}_i - \mathbf{e}_i \in \mathbb{R}^N$ . This enables linear constraints  $\pm r_j \leq \rho, \forall j$ .

We now rewrite the set of linear constraints,  $\mathbf{C}\mathbf{l}_i - \mathbf{r} = \mathbf{e}_i$ ,  $-\mathbf{r} \leq \rho \mathbf{1}_N$ ,  $\mathbf{r} \leq \rho \mathbf{1}_N$ ,  $\tilde{\mathbf{l}} - \mathbf{l}_i \geq \mathbf{0}$ ,  $\tilde{\mathbf{l}} + \mathbf{l}_i \geq \mathbf{0}$ ,  $\mathbf{S}^i \mathbf{l}_i \leq \mathbf{0}$ , into the following aggregate equality constraint:

$$\underbrace{\begin{bmatrix} \mathbf{0}_{N,N} & \mathbf{C} & -\mathbf{I}_N & & \\ \mathbf{0}_{N,N} & \mathbf{0}_{N,N} & \mathbf{I}_N & & \\ \mathbf{0}_{N,N} & \mathbf{0}_{N,N} & -\mathbf{I}_N & & \\ \mathbf{I}_N & -\mathbf{I}_N & \mathbf{0}_{N,N} & & \\ \mathbf{I}_N & \mathbf{I}_N & \mathbf{0}_{N,N} & & \\ \mathbf{0}_{N,N} & -\mathbf{S}^i & \mathbf{0}_{N,N} & & \end{bmatrix}}_{\mathbf{A}} \begin{bmatrix} \tilde{\mathbf{l}} \\ \mathbf{r} \\ \mathbf{q} \end{bmatrix} = \underbrace{\begin{bmatrix} \mathbf{e}_i \\ -\rho \mathbf{1}_N \\ -\rho \mathbf{1}_N \\ \mathbf{0}_N \\ \mathbf{0}_N \\ \mathbf{0}_N \end{bmatrix}}_{\mathbf{b}} \quad (19)$$

where  $\mathbf{q} \geq \mathbf{0}_{5N} \in \mathbb{R}^{5N}$  is a non-negative *slack variable*, so that we can convert inequality constraints to equality constraints. The elements of  $\mathbf{S}^i$  are initialized as in Section IV-D. Note that aggregate matrix  $\mathbf{A}$  is sparse except for  $\mathbf{C}$  (to be further discussed in Section V-C).

For notation convenience, define *main variable*  $\mathbf{x} \triangleq [\tilde{\mathbf{l}}; \mathbf{l}_i; \mathbf{r}] \in \mathbb{R}^{3N}$  and *cost vector*  $\mathbf{c} \triangleq [\mathbf{1}_N; \mathbf{0}_{2N}] \in \mathbb{R}^{3N}$ . We can rewrite the objective as  $\mathbf{c}^\top \mathbf{x}$ . The resulting LP in standard form is

$$\min_{\mathbf{x}, \mathbf{q}} \mathbf{c}^\top \mathbf{x}, \quad \text{s.t. } \mathbf{A} \begin{bmatrix} \mathbf{x} \\ \mathbf{q} \end{bmatrix} = \mathbf{b}, \quad \mathbf{q} \geq \mathbf{0}_{5N}. \quad (20)$$

### B. Fast Optimization via ADMM

We solve LP in standard form (20) efficiently by tailoring an ADMM-based method [30]. We first define a convex but non-differentiable (non-smooth) *indicator function*:

$$g(\mathbf{q}) = \begin{cases} 0 & \text{if } q_j \geq 0, \forall j \\ \infty & \text{o.w.} \end{cases}. \quad (21)$$

Next, to split the objective into two parts, we introduce *auxiliary variable*  $\tilde{\mathbf{q}} \in \mathbb{R}^{5N}$  and rewrite optimization (20):

$$\begin{aligned} \min_{\mathbf{x}, \mathbf{q}, \tilde{\mathbf{q}}} \quad & \mathbf{c}^\top \mathbf{x} + g(\tilde{\mathbf{q}}) \\ \text{s.t.} \quad & \underbrace{\begin{bmatrix} \mathbf{A} & & \\ \mathbf{0}_{5N,3N} & \mathbf{I}_{5N} & -\mathbf{I}_{5N} \end{bmatrix}}_{\mathbf{B}} \begin{bmatrix} \mathbf{x} \\ \mathbf{q} \\ \tilde{\mathbf{q}} \end{bmatrix} = \begin{bmatrix} \mathbf{b} \\ \mathbf{0}_{5N} \end{bmatrix}. \end{aligned} \quad (22)$$

We can now rewrite (22) into an unconstrained version using the augmented Lagrangian method [60] as

$$\begin{aligned} \min_{\mathbf{x}, \mathbf{q}, \tilde{\mathbf{q}}} \quad & \mathbf{c}^\top \mathbf{x} + g(\tilde{\mathbf{q}}) + \boldsymbol{\mu}^\top \left( \mathbf{B} \begin{bmatrix} \mathbf{x} \\ \mathbf{q} \\ \tilde{\mathbf{q}} \end{bmatrix} - \begin{bmatrix} \mathbf{b} \\ \mathbf{0}_{5N} \end{bmatrix} \right) \\ & + \frac{\gamma}{2} \left\| \mathbf{B} \begin{bmatrix} \mathbf{x} \\ \mathbf{q} \\ \tilde{\mathbf{q}} \end{bmatrix} - \begin{bmatrix} \mathbf{b} \\ \mathbf{0}_{5N} \end{bmatrix} \right\|_2^2 \end{aligned} \quad (23)$$

where  $\boldsymbol{\mu} \in \mathbb{R}^{11N}$  is the Lagrange multiplier vector, and  $\gamma > 0$  is a non-negative scalar parameter.

1) *Optimizing Main Variables*: We minimize the unconstrained objective (23) alternately as follows. At iteration  $t$ , when  $\tilde{\mathbf{q}}^t$  is fixed, the optimization for  $\mathbf{x}^{t+1}$  and  $\mathbf{q}^{t+1}$  becomes

$$\begin{aligned} \min_{\mathbf{x}, \mathbf{q}} \quad & \mathbf{c}^\top \mathbf{x} + \boldsymbol{\mu}^\top \left( \mathbf{B} \begin{bmatrix} \mathbf{x} \\ \mathbf{q} \\ \tilde{\mathbf{q}}^t \end{bmatrix} - \begin{bmatrix} \mathbf{b} \\ \mathbf{0}_{5N} \end{bmatrix} \right) \\ & + \frac{\gamma}{2} \left\| \mathbf{B} \begin{bmatrix} \mathbf{x} \\ \mathbf{q} \\ \tilde{\mathbf{q}}^t \end{bmatrix} - \begin{bmatrix} \mathbf{b} \\ \mathbf{0}_{5N} \end{bmatrix} \right\|_2^2. \end{aligned} \quad (24)$$

The solution to this convex and smooth quadratic optimization can be obtained by solving a linear system:

$$\begin{aligned} \gamma \left( \mathbf{A}^\top \mathbf{A} + \underbrace{\begin{bmatrix} \mathbf{0}_{3N,3N} & \mathbf{0}_{3N,5N} \\ \mathbf{0}_{5N,3N} & \mathbf{I}_{5N} \end{bmatrix}}_{\boldsymbol{\Psi}} \right) \begin{bmatrix} \mathbf{x}^{t+1} \\ \mathbf{q}^{t+1} \end{bmatrix} = \\ \gamma \left( \begin{bmatrix} \mathbf{0}_{3N} \\ \tilde{\mathbf{q}} \end{bmatrix} - \mathbf{A}^\top \mathbf{b} \right) - \begin{bmatrix} \mathbf{c} \\ \mathbf{0}_{5N} \end{bmatrix} - \mathbf{A}^\top \boldsymbol{\mu}_1 - \begin{bmatrix} \mathbf{0}_{3N} \\ \boldsymbol{\mu}_2 \end{bmatrix} \end{aligned} \quad (25)$$

where  $\boldsymbol{\mu}_1 \in \mathbb{R}^{6N}$  and  $\boldsymbol{\mu}_2 \in \mathbb{R}^{5N}$  are the multiplier sub-vectors such that  $\boldsymbol{\mu} = [\boldsymbol{\mu}_1; \boldsymbol{\mu}_2]$ . See Appendix A for a derivation.

**Complexity**: Linear system (25) can be solved efficiently using *conjugate gradient* (CG) with complexity  $\mathcal{O}(\text{nnz}(\boldsymbol{\Psi})\sqrt{\kappa(\boldsymbol{\Psi})}/\log(\epsilon))$ , where  $\text{nnz}(\boldsymbol{\Psi})$  is the number of non-zero entries in matrix  $\boldsymbol{\Psi}$ ,  $\kappa(\boldsymbol{\Psi}) = \frac{\lambda_{\max}(\boldsymbol{\Psi})}{\lambda_{\min}(\boldsymbol{\Psi})}$  is the *condition number* of  $\boldsymbol{\Psi}$ ,  $\lambda_{\max}(\boldsymbol{\Psi})$  and  $\lambda_{\min}(\boldsymbol{\Psi})$  are the respective largest and smallest eigenvalues of  $\boldsymbol{\Psi}$ , and  $\epsilon$  is the convergence threshold of the gradient search [61].  $\kappa(\boldsymbol{\Psi})$  is reasonably small in practice. Assuming  $\epsilon$  is set reasonably, CG's execution time is  $\mathcal{O}(\text{nnz}(\boldsymbol{\Psi})) = \mathcal{O}(N^2)$  due to dense  $N$ -by- $N$  sample covariance matrix  $\mathbf{C}$  in  $\mathbf{A}$  in (19).

2) *Optimizing Auxiliary Variable*: Fixing computed  $\mathbf{x}^{t+1}$  and  $\mathbf{q}^{t+1}$ , the optimization (23) for  $\tilde{\mathbf{q}}^{t+1}$  at iteration  $t$  becomes

$$\begin{aligned} \min_{\tilde{\mathbf{q}}} \quad & g(\tilde{\mathbf{q}}) + \boldsymbol{\mu}_2^\top \left( \begin{bmatrix} \mathbf{I}_{5N} & -\mathbf{I}_{5N} \end{bmatrix} \begin{bmatrix} \mathbf{q}^{t+1} \\ \tilde{\mathbf{q}} \end{bmatrix} \right) \\ & + \frac{\gamma}{2} \left\| \begin{bmatrix} \mathbf{I}_{5N} & -\mathbf{I}_{5N} \end{bmatrix} \begin{bmatrix} \mathbf{q}^{t+1} \\ \tilde{\mathbf{q}} \end{bmatrix} \right\|_2^2. \end{aligned} \quad (26)$$

The solution is a *separable* thresholding operation. Specifically, at iteration  $t$ , we compute  $\tilde{\mathbf{q}}^{t+1}$  as

$$q_j^{t+1} = \begin{cases} 0 & \text{if } q_j^{t+1} + \frac{1}{\gamma} \mu_{2,j}^t < 0 \\ q_j^{t+1} + \frac{1}{\gamma} \mu_{2,j}^t & \text{o.w.} \end{cases}. \quad (27)$$

See Appendix B for a derivation.

**Complexity**: Because (27) is a simple addition executed entry-by-entry for  $\mathcal{O}(N)$  entries, the complexity is  $\mathcal{O}(N)$ .

3) *Updating Lagrange Multipliers*: After computing  $\mathbf{x}^{t+1}$ ,  $\mathbf{q}^{t+1}$  and  $\tilde{\mathbf{q}}^{t+1}$ , Lagrange multiplier vector  $\boldsymbol{\mu}^{t+1}$  can be updated at iteration  $t$  in the usual manner in ADMM [60]:

$$\boldsymbol{\mu}^{t+1} = \boldsymbol{\mu}^t + \gamma \left( \mathbf{B} \begin{bmatrix} \mathbf{x}^{t+1} \\ \mathbf{q}^{t+1} \\ \tilde{\mathbf{q}}^{t+1} \end{bmatrix} - \begin{bmatrix} \mathbf{b} \\ \mathbf{0}_{5N} \end{bmatrix} \right). \quad (28)$$

**Complexity**: (28) requires one matrix-vector multiplication and simple vector additions, where  $\text{nnz}(\mathbf{B}) = \mathcal{O}(N^2)$ , again due to dense  $N$ -by- $N$  matrix  $\mathbf{C}$  in  $\mathbf{A}$  in (19). Thus, the complexity is  $\mathcal{O}(N^2)$ .



TABLE II  
SYNTHETIC EXPERIMENT RESULTS

$K \gg N$ setting ( $N = 50, K = 500$ )														
	Proposed		GLASSO						CLIME					
	–		Min		Max		Greed		Min		Max		Greed	
Noise variance	0	0.25	0	0.25	0	0.25	0	0.25	0	0.25	0	0.25	0	0.25
FM $\uparrow$	<b>0.668</b>	<b>0.583</b>	0.494	0.422	0.489	0.431	0.517	0.463	0.462	0.429	0.464	0.436	0.496	0.464
RE $\downarrow$	<b>0.279</b>	<b>0.478</b>	0.312	0.487	0.314	0.487	0.309	0.485	0.359	0.492	0.358	0.492	0.355	0.490
$K \ll N$ setting ( $N = 100, K = 50$ )														
Noise level	0	0.25	0	0.25	0	0.25	0	0.25	0	0.25	0	0.25	0	0.25
FM $\uparrow$	<b>0.387</b>	<b>0.303</b>	0.202	0.188	0.202	0.188	0.091	0.086	0.131	0.158	0.130	0.163	0.105	0.096
AE $\downarrow$	<b>1.003</b>	1.147	1.653	1.290	1.649	1.291	1.651	1.292	1.036	<b>1.077</b>	1.039	1.077	1.063	1.102

Synthetic graph signals were generated following the Gaussian Markov Random Field (GMRF) model as  $\mathbf{x}^k \sim \mathcal{N}(\mathbf{0}_N, (\mathcal{L}^b)^{-1})$ . We generated  $K = 500$  observations for the graph with  $N = 50$  (corresponding to the  $K \gg N$  case), and  $K = 50$  observations for the graph with  $N = 100$  (corresponding to the  $K \ll N$  case). Along with the noiseless experiment, we also conducted an experiment where signals were corrupted by additive white Gaussian noise with standard deviation  $\sigma = 0.25$ .

The performance of our algorithm is compared against several two-step graph balancing approaches, i.e., a precision matrix estimation followed by a graph balancing step. We employed CLIME [28] or GLASSO [24] as the baseline precision matrix estimation methods. The three variants of graph balancing methods were;

**MinCut Balancing (Min) [27]:** Nodes were polarized based on the min-cut of positive edges, and inconsistent edges were removed.

**MaxCut Balancing (Max) [27]:** Nodes were polarized based on the max-cut of negative edges, and inconsistent edges were removed.

**Greedy Balancing (Greed) [22]:** A polarized set was initialized by polarizing a random node to 1, then nodes connected to the set were greedily polarized one by one, keeping the edge with the largest weight magnitude and removing the rest in each polarization.

As a result, alternative methods have six configurations.

2) *Results:* Tables II summarize the results. The values are the average over 30 independent runs. We observe that the proposed method outperforms alternative approaches in both of the  $K \gg N$  and  $K \ll N$  cases. For  $K \ll N$ , the proposed method performs better than the other methods in most cases.

### B. Graph Signal Restoration on Real-World Datasets

We next evaluate the proposed balanced graph learning method on real-world datasets. Since we do not have the ground-truth graphs in this setting, we demonstrate the performance via graph signal denoising and interpolation. For both tasks, we employ graph filters and GNNs, which require a positive graph kernel as input, to show that they can be reused on balanced signed graphs.

For competing methods, we estimated two signed graphs using GLASSO and CLIME, then constructed a balanced signed graph using *Greed* [22] as in the previous subsection. We also performed balanced signature graph learning (BsigGL) [23], a recently proposed balanced graph learning method. We also

compared the performance against positive graphs. For positive graph learning, we followed two different formulations in [34]. The first estimated a combinatorial graph Laplacian (CGL):

$$\min_{\mathbf{L}} \text{Tr}(\mathbf{L}\mathbf{K}) - \log |\mathbf{L}| \quad \text{subject to } \mathbf{L} \in \mathcal{L}_c(\mathbf{A}). \quad (36)$$

The second estimated generalized graph Laplacian (GGL):

$$\min_{\mathbf{L}} \text{Tr}(\mathbf{L}\mathbf{K}) - \log |\mathbf{L}| \quad \text{subject to } \mathbf{L} \in \mathcal{L}_g(\mathbf{A}) \quad (37)$$

where  $\mathbf{K} = \mathbf{C} + \mathbf{F}$  is the regularization matrix defined as  $\mathbf{F} = \alpha \mathbf{2}(\mathbf{I} - \mathbf{1}\mathbf{1}^T)$ ,  $\mathbf{A}$  is a connectivity matrix, and  $\mathcal{L}_c$  and  $\mathcal{L}_g$  are feasible sets for CGLs and GGLs, respectively. Here we set  $\mathbf{A} = \mathbf{1}\mathbf{1}^T - \mathbf{I}$  because the true connectivity is unknown.

1) *Datasets:* The specifications of the real-world datasets used in this experiment are listed as follows.

- 1) *United States Senate*<sup>7</sup> (*USS, Ternary*): The dataset consists of US Senate voting records from 115th and 116th Congress in 2005-2021 and contains voting records of 100 senators who voted in 1320 elections.
- 2) *Canadian Parliament Voting Records*<sup>8</sup> (*CPV, Ternary*): The dataset consists of Canadian Parliament voting records from the 38th parliament in 2005 and contains voting records of 340 constituencies voted in 3154 elections.
- 3) *Hourly Air Pressures in Japan*<sup>9</sup> (*APJ, Real*): This dataset consists of hourly air pressure records from 48 weather stations in Japan from March 2022 to May 2022. The number of observations is  $K = 2016$ .
- 4) *Monthly Japanese Industrial Sales*<sup>10</sup> (*JPS, Real*): This dataset consists of monthly industrial sales from 29 industries in Japan from December 2020 to December 2023. The total number of observations is  $K = 37$ . We normalized the sales values of each industry and ignored any industry that had a near-zero correlation coefficient (less than 0.01) with any other industry.

For the two voting datasets, USS and CPV, the votes were recorded as  $-1$  for *no* and  $1$  for *yes* and  $0$  for *abstain/absent*. We removed any sample with all *yes* or *no* votes, or with more than 50% *abstain/absent* to emphasize the polarity in the dataset. We also ignored constituencies with less than 800 voting records for the CPV dataset. For the APJ dataset, the data were normalized to be zero-mean and unit variance to emphasize the spatial variance.

<sup>7</sup><https://www.congress.gov/roll-call-votes>

<sup>8</sup><https://www.ourcommons.ca/members/en/votes>

<sup>9</sup><https://www.data.jma.go.jp/stats/etrn/index.php>

<sup>10</sup><https://www.e-stat.go.jp/>

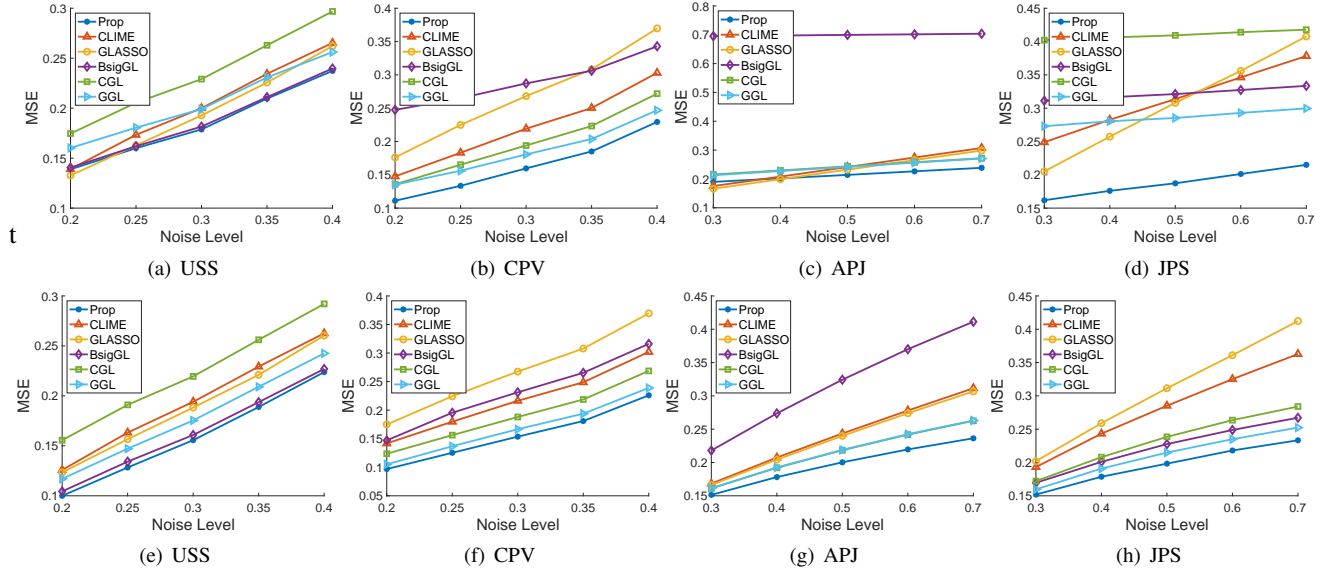


Fig. 3. Results of signal denoising using estimated graph Laplacians. Figures in the top row are the results of graph low-pass filtering (BL), and figures in the bottom row are the results of graph spectral wavelets (SGW). The mean squared errors (MSE) are averaged over 50 independent runs.

TABLE III  
MSES FOR DENOISING WITH GRAPH NEURAL NETWORKS

Dataset	Model	Method	0.20	0.25	0.30	0.35	0.40	Dataset	Model	Method	0.30	0.40	0.50	0.60	0.70
USS	GCN	Prop	0.084	0.096	0.105	0.114	0.127	JPS	GCN	Prop	<b>0.069</b>	0.101	<b>0.132</b>	<b>0.145</b>	<b>0.193</b>
		BsigGL	0.104	0.104	0.112	0.118	0.125			BsigGL	0.100	0.138	0.183	0.201	0.237
		CGL	0.107	0.119	0.129	0.140	0.151			CGL	0.103	0.132	0.139	0.177	0.208
		GGL	<b>0.079</b>	<b>0.093</b>	<b>0.092</b>	<b>0.108</b>	<b>0.133</b>			GGL	<u>0.072</u>	<b>0.091</b>	<u>0.123</u>	<u>0.160</u>	<u>0.208</u>
	GAT	Prop	<b>0.104</b>	<u>0.128</u>	<b>0.131</b>	<b>0.139</b>	0.159		BsigGL	0.098	0.138	<b>0.161</b>	<b>0.188</b>	<b>0.214</b>	
		BsigGL	0.116	<b>0.126</b>	<u>0.137</u>	<u>0.135</u>	<b>0.158</b>		CGL	0.109	0.165	0.240	0.258	<u>0.297</u>	
CPV	GCN	CGL	0.127	0.186	0.203	0.272	0.312	GCN	BsigGL	0.109	0.156	0.208	0.242	0.308	
		GGL	<u>0.112</u>	0.138	0.145	0.148	0.186		CGL	<u>0.095</u>	0.156	0.208	0.242	0.308	
		Prop	<b>0.100</b>	<b>0.096</b>	<b>0.092</b>	<b>0.107</b>	<b>0.115</b>		GGL	<b>0.091</b>	<b>0.128</b>	<u>0.167</u>	<u>0.233</u>	0.302	
		BsigGL	0.123	0.121	0.157	0.180	0.203		Prop	<b>0.097</b>	<b>0.084</b>	<b>0.097</b>	<b>0.126</b>	<b>0.143</b>	
	GAT	CGL	0.166	0.177	0.202	0.222	0.247	BsigGL	0.114	0.099	0.114	0.158	0.180		
		GGL	0.109	0.108	0.117	0.128	0.136	CGL	0.105	0.085	0.105	0.138	0.161		
APJ	GCN	GGL	<b>0.122</b>	<b>0.146</b>	<b>0.159</b>	<b>0.181</b>	<u>0.220</u>	GGL	<u>0.104</u>	0.089	0.104	0.131	<u>0.159</u>		
		Prop	0.191	0.235	0.301	0.337	0.371	Prop	0.080	0.122	0.151	0.185	0.232		
		BsigGL	0.168	0.180	0.221	0.251	0.292	BsigGL	0.094	0.135	0.220	0.288	0.395		
		CGL	0.141	0.151	0.191	0.194	<b>0.219</b>	CGL	<u>0.071</u>	<b>0.093</b>	<u>0.127</u>	<u>0.151</u>	<u>0.200</u>		
GAT	CGL	0.168	0.180	0.221	0.251	0.292	GGL	<b>0.059</b>	<u>0.093</u>	<b>0.123</b>	<b>0.156</b>	<b>0.187</b>			
	GGL	0.141	0.151	0.191	0.194	<b>0.219</b>	Prop	0.080	0.122	0.151	0.185	0.232			

For all real-world datasets, we randomly selected 90% of the sample to compute the sample covariance matrix as  $\mathbf{C} = (1/N)\mathbf{X}\mathbf{X}^T + \xi\mathbf{I}$  where  $\xi$  is a small constant to ensure  $\mathbf{C}$  is non-singular. Then, the remaining 10% were used for restoration tasks. For the JPS dataset, we only had  $K_{\text{sample}} = 4$  test samples, so we generated 10 different noise realizations to make sure all datasets had at least  $K_{\text{sample}} > N/2$  test samples.

2) *Signal Denoising Settings*: The test data in the real-valued datasets are contaminated with an additive white Gaussian noise (AWGN) with  $\sigma = \{0.3, 0.4, 0.5, 0.6, 0.7\}$ . For the ternary-valued datasets (USS and CPV), we dropped signal values of  $n_p N$  nodes from the test data, where  $n_p = \{0.2, 0.25, 0.3, 0.35, 0.4\}$  to represent a Bernoulli noise.

For positive graph signal denoising, we employed a bandlimited graph low-pass filter (BL), spectral graph wavelets (SGW) [11], graph convolutional net (GCN) [4], and graph attention net (GAT) [33]. The learned balanced signed graph Laplacian  $\mathcal{L}^b$  was similarity-transformed (via matrix  $\mathbf{T}$  in (4)) to a positive graph Laplacian  $\mathcal{L}^+$  as a kernel for the denoising algorithms. Each observed noisy signal was also similarity-transformed via  $\mathbf{T}$  for processing on positive graph  $\mathcal{G}^+$ . For BL, we used a

filter that preserves the low-frequency band  $[0, 0.3\lambda_{\max}]$ , where  $\lambda_{\max}$  was the maximum eigenvalue of the graph Laplacian. For SGW, we designed the Mexican hat wavelet filter bank for range  $[0, \lambda_{\max}]$ . The number of frames was set to 7. For GCN and GAT, we followed the untrained GNN implementation in [63] for signal denoising on positive graphs.

3) *Signal Interpolation Settings*: The test data were interpolated from a randomly sampled subset with sample rates  $r = \{0.10, 0.15, 0.20, 0.25, 0.30\}$ . For signal interpolation, we followed the formulation in [32]. Specifically, [32] requires a positive graph kernel and interpolates missing samples using an upsampling/low-pass filtering procedure. Here, the graph low-pass filter with a cutoff frequency of  $\lambda_{\text{cut}} = 0.3\lambda_{\max}$  is defined as  $f((1 - \lambda_i)/\lambda_{\text{cut}})$  where

$$f(x) = \begin{cases} 0 & \text{if } x \leq 0, \\ \frac{\exp(-1/x)}{\exp(-1/x) + \exp(-1/(1-x))} & \text{if } x \in (0, 1), \\ 1 & \text{if } x \geq 1. \end{cases} \quad (38)$$

Again, the learned balanced graph Laplacian was similarity-transformed into a positive graph before being used as a kernel for the interpolation algorithm.

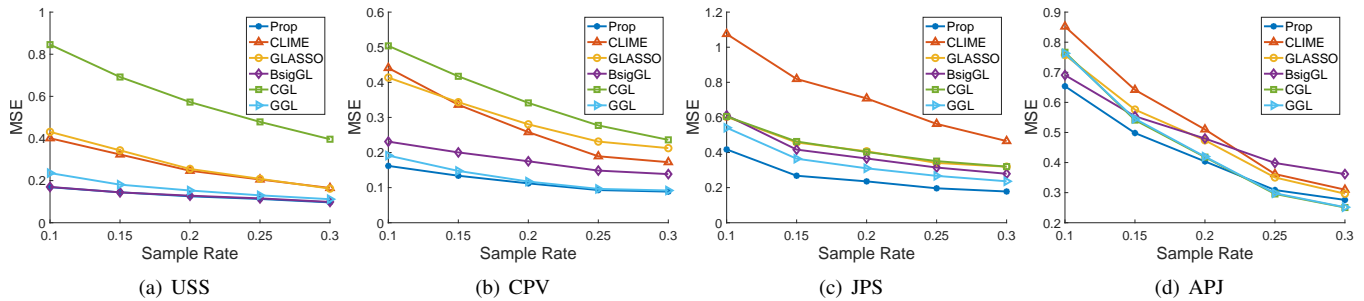


Fig. 4. Results of signal interpolation using estimated graph Laplacians. The mean squared errors (MSE) are averaged over 50 independent runs.

4) *Results:* Figs. 3 and 4 show the mean squared errors (MSE) of the denoised and interpolated signals by filtering-based methods, respectively. The denoising results with GNNs are also presented in Table III, where the best results are shown in bold, and the second-best results are underlined.

From Fig. 3, we observe that the graph learned with the proposed method consistently achieves the lowest MSEs in most cases. While BsigGL is comparable to the proposed method for the USS data, its MSEs are larger than the other methods for the other datasets. Table III shows that the proposed method consistently performs well in all datasets and noise levels.

The results on the positive graphs and the balanced signed graphs for the USS and APJ datasets are sometimes similar. This implies that the nodes in the USS and APJ datasets tend to form separate clusters according to their polarity. This behavior is intuitive: in the USS dataset, senators from opposing parties often cast opposing votes, which naturally induces polarization. Similarly, in the APJ dataset, springtime pressure systems in Japan typically propagate from west to east, leading to spatial separation between high and low pressure regions. In both cases, the dominant structure can be effectively captured by clusters of positively correlated nodes. Consequently, a simple positive graph filter can sufficiently recover the signals, resulting in performance comparable to that of the proposed approach. In contrast, the cluster structures in the CPV and JPS datasets are not as clear as those in the USS and APJ datasets. The Canadian parliament consists of five distinct political groups, including parties that occupy middle positions between liberal and conservative ideologies, and industries in Japan do not always rise or fall in a polarized manner.

To investigate structural differences, we compare the spectra of the graphs obtained by the proposed method and those by the alternative methods. Fig. 5 shows the cumulative spectra for the first 30% eigenvalues of learned graphs against their indices. As can be seen from Figs. 5(a) and (d), the spectra of the proposed signed graphs are similar to those of BsigGL and GGL on USS, and are close to the positive graphs on APJ. This spectral similarity indicates that the graphs are nearly isospectral [64], which explains the comparable signal restoration performance for these polarized datasets. Conversely, distinct spectral profiles in CPV and JPS correspond to the mixture of positive and negative relationships, where our method shows advantages.

Overall, our approach demonstrates consistent effectiveness across all datasets, adaptively handling both polarized and complex multi-faceted signal relationships.

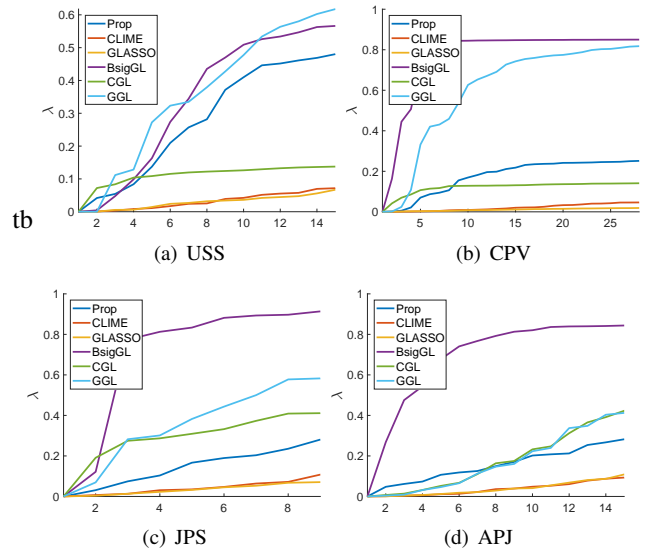


Fig. 5. First 30% eigenvalues of estimated graph Laplacians (rescaled to  $[0, 1]$ ). The horizontal axis represents the index of eigenvalues.

## VII. CONCLUSION

We propose an efficient algorithm to learn a balanced signed graph directly from data. We augment a previous linear programming (LP) based sparse inverse covariance matrix estimation method called CLIME [28] with additional linear constraints to enforce graph balance. For each sparse LP that targets a column  $\mathbf{l}_i$  in balanced graph Laplacian  $\mathcal{L}^b$ , we adapt ADMM to solve  $\mathbf{l}_i$  efficiently. We derive a suitable CLIME parameter  $\rho$  specifying sparsity level based on the Hannan-Quinn information criterion and a minimum feasibility criterion. We theoretically prove algorithm convergence to a local minimum. Extensive experiments show that our balanced graph learning method enables reuse of spectral filters / GCNs for positive graphs and outperforms previous learning methods.

## REFERENCES

- [1] D. I. Shuman, S. K. Narang, P. Frossard, A. Ortega, and P. Vandergheynst, "The emerging field of signal processing on graphs: Extending high-dimensional data analysis to networks and other irregular domains," *IEEE Signal Process. Mag.*, vol. 30, no. 3, pp. 83–98, 2013.
- [2] A. Ortega, P. Frossard, J. Kovačević, J. M. F. Moura, and P. Vandergheynst, "Graph Signal Processing: Overview, Challenges, and Applications," *Proc. IEEE*, vol. 106, no. 5, pp. 808–828, 2018.
- [3] Y. Tanaka, Y. C. Eldar, A. Ortega, and G. Cheung, "Sampling Signals on Graphs: From Theory to Applications," *IEEE Signal Process. Mag.*, vol. 37, no. 6, pp. 14–30, 2020.

- [4] T. N. Kipf and M. Welling, "Semi-supervised classification with graph convolutional networks," in *Proceedings of the 5th International Conference on Learning Representations (ICLR)*, 2017.
- [5] J. Friedman, T. Hastie, and R. Tibshirani, "Sparse inverse covariance estimation with the graphical lasso," *Biostatistics*, vol. 9, no. 3, pp. 432–441, 2008.
- [6] V. Kalofolias, "How to Learn a Graph from Smooth Signals," in *Proc. 19th Int. Conf. Artif. Intell. Stat.* PMLR, 2016, pp. 920–929.
- [7] D. Thanou, X. Dong, D. Kressner, and P. Frossard, "Learning heat diffusion graphs," *IEEE Trans. Signal Inf. Process. Netw.*, vol. 3, pp. 484–499, 2016.
- [8] M. Onuki, S. Ono, M. Yamagishi, and Y. Tanaka, "Graph Signal Denoising via Trilateral Filter on Graph Spectral Domain," *IEEE Trans. Signal Inf. Process. Netw.*, vol. 2, no. 2, pp. 137–148, 2016.
- [9] J. Pang and G. Cheung, "Graph Laplacian regularization for inverse imaging: Analysis in the continuous domain," in *IEEE Trans. Image Process.*, vol. 26, no.4, April 2017, pp. 1770–1785.
- [10] D. I. Shuman, "Localized spectral graph filter frames: A unifying framework, survey of design considerations, and numerical comparison," *IEEE Signal Processing Magazine*, vol. 37, no. 6, pp. 43–63, 2020.
- [11] D. K. Hammond, P. Vandergheynst, and R. Gribonval, "Wavelets on graphs via spectral graph theory," *Applied and Computational Harmonic Analysis*, vol. 30, no. 2, pp. 129–150, 2011.
- [12] A. Gadde, S. K. Narang, and A. Ortega, "Bilateral filter: Graph spectral interpretation and extensions," in *2013 IEEE International Conference on Image Processing*, 2013, pp. 1222–1226.
- [13] S. Chen, A. Sandryhaila, J. M. F. Moura, and J. Kovačević, "Signal recovery on graphs: Variation minimization," *IEEE Transactions on Signal Processing*, vol. 63, no. 17, pp. 4609–4624, 2015.
- [14] X. Liu, G. Cheung, X. Ji, D. Zhao, and W. Gao, "Graph-based joint dequantization and contrast enhancement of poorly lit jpeg images," *IEEE Transactions on Image Processing*, vol. 28, no. 3, pp. 1205–1219, 2019.
- [15] Y. Yazaki, Y. Tanaka, and S. H. Chan, "Interpolation and denoising of graph signals using plug-and-play admm," in *ICASSP 2019 - 2019 IEEE International Conference on Acoustics, Speech and Signal Processing (ICASSP)*, 2019, pp. 5431–5435.
- [16] M. Nagahama, K. Yamada, Y. Tanaka, S. H. Chan, and Y. C. Eldar, "Graph signal restoration using nested deep algorithm unrolling," *IEEE Transactions on Signal Processing*, vol. 70, pp. 3296–3311, 2022.
- [17] Y. Hou, J. Li, and Y. Pan, "On the Laplacian Eigenvalues of Signed Graphs," *Linear Multilinear Algebra*, vol. 51, no. 1, pp. 21–30, 2003.
- [18] L. Wu, X. Ying, X. Wu, A. Lu, and Z.-H. Zhou, "Spectral Analysis of k-Balanced Signed Graphs," in *Adv. Knowl. Discov. Data Min.*, ser. Lecture Notes in Computer Science, J. Z. Huang, L. Cao, and J. Srivastava, Eds. Berlin, Heidelberg: Springer, 2011, pp. 1–12.
- [19] J. Kunegis, S. Schmidt, A. Lommatzsch, J. Lerner, E. W. De Luca, and S. Albayrak, "Spectral Analysis of Signed Graphs for Clustering, Prediction and Visualization," in *Proceedings of the 2010 SIAM International Conference on Data Mining (SDM)*, ser. Proceedings. Society for Industrial and Applied Mathematics, 2010, pp. 559–570.
- [20] T. Dittrich and G. Matz, "Signal Processing on Signed Graphs: Fundamentals and Potentials," *IEEE Signal Process. Mag.*, vol. 37, no. 6, pp. 86–98, 2020.
- [21] E. B. Davies, J. Leydold, and P. F. Stadler, "Discrete nodal domain theorems," *Elsevier Linear Algebra and its Application*, 2000.
- [22] C. Dinesh, G. Cheung, S. Bagheri, and I. V. Bajić, "Efficient signed graph sampling via balancing & gershgorin disc perfect alignment," *IEEE Transactions on Pattern Analysis and Machine Intelligence*, vol. 47, no. 4, pp. 2330–2348, 2025.
- [23] G. Matz, C. Verardo, and T. Dittrich, "Efficient learning of balanced signature graphs," in *ICASSP 2023 - 2023 IEEE International Conference on Acoustics, Speech and Signal Processing (ICASSP)*, 2023, pp. 1–5.
- [24] R. Mazumder and T. Hastie, "The graphical lasso: New insights and alternatives," *Electron J Stat*, vol. 6, pp. 2125–2149, 2012.
- [25] J. Akiyama, D. Avis, V. Chvátal, and H. Era, "Balancing signed graphs," *Discrete Applied Mathematics*, vol. 3, no. 4, pp. 227–233, 1981.
- [26] C. Dinesh, S. Bagheri, G. Cheung, and I. V. Bajić, "Linear-Time Sampling on Signed Graphs Via Gershgorin Disc Perfect Alignment," in *ICASSP 2022 - 2022 IEEE Int. Conf. Acoust. Speech Signal Process.* ICASSP, 2022, pp. 5942–5946.
- [27] H. Yokota, J. Hara, Y. Tanaka, and G. Cheung, "Signed graph balancing with graph cut," in *2023 31st European Signal Processing Conference (EUSIPCO)*, 2023, pp. 1853–1857.
- [28] T. Cai, W. Liu, and X. Luo, "A constrained  $\ell_1$  minimization approach to sparse precision matrix estimation," *Journal of the American Statistical Association*, vol. 106, no. 494, pp. 594–607, 2011.
- [29] F. Harary, "On the notion of balance of a signed graph," *Mich. Math. J.*, vol. 2, no. 2, pp. 143–146, 1953.
- [30] S. Wang and N. Shroff, "A new alternating direction method for linear programming," in *Advances in Neural Information Processing Systems*, I. Guyon, U. V. Luxburg, S. Bengio, H. Wallach, R. Fergus, S. Vishwanathan, and R. Garnett, Eds., vol. 30. Curran Associates, Inc., 2017. [Online]. Available: [https://proceedings.neurips.cc/paper\\_files/paper/2017/file/c4b31ce7d95c75ca70d50c19aef08bf1-Paper.pdf](https://proceedings.neurips.cc/paper_files/paper/2017/file/c4b31ce7d95c75ca70d50c19aef08bf1-Paper.pdf)
- [31] E. J. Hannan and B. G. Quinn, "The determination of the order of an autoregression," *Journal of the Royal Statistical Society. Series B (Methodological)*, vol. 41, no. 2, pp. 190–195, 1979.
- [32] I. Pesenson, "Variational Splines and Paley–Wiener Spaces on Combinatorial Graphs," *Constr Approx*, vol. 29, no. 1, pp. 1–21, 2009.
- [33] P. Velickovic, G. Cucurull, A. Casanova, A. Romero, P. Lio, Y. Bengio et al., "Graph attention networks," in *Proceedings of the 6th International Conference on Learning Representations (ICLR)*, 2018.
- [34] H. E. Egilmez, E. Pavez, and A. Ortega, "Graph Learning From Data Under Laplacian and Structural Constraints," *IEEE J. Sel. Top. Signal Process.*, vol. 11, no. 6, pp. 825–841, 2017.
- [35] S. Kumar, J. Ying, J. V. d. M. Cardoso, and D. P. Palomar, *Structured graph learning via laplacian spectral constraints*. Red Hook, NY, USA: Curran Associates Inc., 2019.
- [36] S. Bagheri, T. T. Do, G. Cheung, and A. Ortega, "Spectral graph learning with core eigenvectors prior via iterative GLASSO and projection," *IEEE Transactions on Signal Processing*, vol. 72, pp. 3958–3972, 2024.
- [37] X. Dong, D. Thanou, P. Frossard, and P. Vandergheynst, "Learning laplacian matrix in smooth graph signal representations," *IEEE Transactions on Signal Processing*, vol. 64, no. 23, pp. 6160–6173, 2016.
- [38] X. Dong, D. Thanou, M. Rabbat, and P. Frossard, "Learning graphs from data: A signal representation perspective," *IEEE Signal Process. Mag.*, vol. 36, no. 3, pp. 44–63, 2019.
- [39] S. Bagheri, G. Cheung, T. Eadie, and A. Ortega, "Joint signal interpolation / time-varying graph estimation via smoothness and low-rank priors," in *ICASSP 2024 - 2024 IEEE International Conference on Acoustics, Speech and Signal Processing (ICASSP)*, 2024, pp. 9646–9650.
- [40] W. Hu, X. Gao, G. Cheung, and Z. Guo, "Feature graph learning for 3d point cloud denoising," *IEEE Transactions on Signal Processing*, vol. 68, pp. 2841–2856, 2020.
- [41] C. Yang, G. Cheung, and W. Hu, "Signed Graph Metric Learning via Gershgorin Disc Perfect Alignment," *IEEE Trans. Pattern Anal. Mach. Intell.*, vol. 44, no. 10, pp. 7219–7234, 2022.
- [42] V. H. T. T. DO, P. Eftekhari, S. A. Hosseini, G. Cheung, and P. Chou, "Interpretable lightweight transformer via unrolling of learned graph smoothness priors," in *Advances in Neural Information Processing Systems*, A. Globerson, L. Mackey, D. Belgrave, A. Fan, U. Paquet, J. Tomczak, and C. Zhang, Eds., vol. 37. Curran Associates, Inc., 2024, pp. 6393–6416. [Online]. Available: [https://proceedings.neurips.cc/paper\\_files/paper/2024/file/0c38f54740062529aa4117a04b583f3c-Paper-Conference.pdf](https://proceedings.neurips.cc/paper_files/paper/2024/file/0c38f54740062529aa4117a04b583f3c-Paper-Conference.pdf)
- [43] C. Tomasi and R. Manduchi, "Bilateral filtering for gray and color images," in *Sixth International Conference on Computer Vision*, 1998, pp. 839–846.
- [44] J. Kunegis, S. Schmidt, A. Lommatzsch, J. Lerner, E. W. D. Luca, and S. Albayrak, "Spectral analysis of signed graphs for clustering, prediction and visualization," in *Proceedings of the 2010 SIAM International Conference on Data Mining (SDM)*, 2010, pp. 559–570. [Online]. Available: <https://epubs.siam.org/doi/abs/10.1137/1.9781611972801.49>
- [45] H. Yokota, H. Higashi, Y. Tanaka, and G. Cheung, "Efficient learning of balanced signed graphs via iterative linear programming," in *ICASSP 2025 - 2025 IEEE International Conference on Acoustics, Speech and Signal Processing (ICASSP)*, 2025, pp. 1–5.
- [46] S. Jiang, Z. Song, O. Weinstein, and H. Zhang, "A faster algorithm for solving general LPs," in *Proceedings of the 53rd Annual ACM SIGACT Symposium on Theory of Computing*, ser. STOC 2021. Association for Computing Machinery, Jun. 2021, pp. 823–832.
- [47] W.-T. Su, G. Cheung, and C.-W. Lin, "Graph Fourier transform with negative edges for depth image coding," in *2017 IEEE International Conference on Image Processing (ICIP)*, 2017, pp. 1682–1686.
- [48] R. S. Varga, *Gershgorin and his circles*. Springer, 2004.
- [49] G. Cheung, E. Magli, Y. Tanaka, and M. K. Ng, "Graph spectral image processing," in *Proceedings of the IEEE*, vol. 106, no.5, May 2018, pp. 907–930.
- [50] C. Dinesh, J. Wang, G. Cheung, and P. Srikantha, "Complex graph Laplacian regularizer for inferencing grid states," in *2023 IEEE International Conference on Communications, Control, and Computing Technologies for Smart Grids (SmartGridComm)*, 2023.

- [51] Z.-q. Luo, W.-k. Ma, A. M.-c. So, Y. Ye, and S. Zhang, "Semidefinite relaxation of quadratic optimization problems," *IEEE Signal Processing Magazine*, vol. 27, no. 3, pp. 20–34, 2010.
- [52] T. Antal, P. L. Krapivsky, and S. Redner, "Dynamics of social balance on networks," *Phys. Rev. E*, vol. 72, no. 3, p. 036121, Sep. 2005.
- [53] J. Hu and W. X. Zheng, "Bipartite consensus for multi-agent systems on directed signed networks," in *52nd IEEE Conference on Decision and Control*, Dec. 2013, pp. 3451–3456.
- [54] C. M. Rawlings and N. E. Friedkin, "The Structural Balance Theory of Sentiment Networks: Elaboration and Test," *American Journal of Sociology*, vol. 123, no. 2, pp. 510–548, Sep. 2017.
- [55] A. Gallo, D. Garlaschelli, R. Lambiotte, F. Saracco, and T. Squartini, "Testing structural balance theories in heterogeneous signed networks," *Commun Phys*, vol. 7, no. 1, pp. 1–13, May 2024.
- [56] F. R. Hampel, E. M. Ronchetti, P. J. Rousseeuw, and W. A. Stahel, *Robust Statistics*. Wiley, 2005.
- [57] H. Akaike, "Information Theory and an Extension of the Maximum Likelihood Principle," in *Selected Papers of Hirotugu Akaike*, E. Parzen, K. Tanabe, and G. Kitagawa, Eds. New York, NY: Springer, 1998, pp. 199–213.
- [58] G. Schwarz, "Estimating the dimension of a model," *The Annals of Statistics*, vol. 6, no. 2, pp. 461–464, 1978.
- [59] K. Yamada and Y. Tanaka, "Graph learning information criterion," in *ICASSP 2022 - 2022 IEEE International Conference on Acoustics, Speech and Signal Processing (ICASSP)*, 2022, pp. 5642–5646.
- [60] S. Boyd, N. Parikh, E. Chu, B. Peleato, and J. Eckstein, *Distributed Optimization and Statistical Learning via the Alternating Direction Method of Multipliers*. Now Foundations and Trends, 2011.
- [61] J. R. Shewchuk, "An introduction to the conjugate gradient method without the agonizing pain," Carnegie Mellon University, USA, Tech. Rep., 1994.
- [62] P. Erdős and A. Rényi, "On random graphs i," *Publicationes Mathematicae Debrecen*, vol. 6, pp. 290–297, 1959.
- [63] S. Rey, S. Segarra, R. Heckel, and A. G. Marques, "Untrained Graph Neural Networks for Denoising," *IEEE Transactions on Signal Processing*, vol. 70, pp. 5708–5723, 2022.
- [64] N. Biggs, *Algebraic graph theory*. Cambridge university press, 1993, no. 67.

augmented Lagrangian term is  $\gamma/2$  times the following:

$$\begin{aligned}
 & (\mathbf{A}\mathbf{y} - \mathbf{b})^\top (\mathbf{A}\mathbf{y} - \mathbf{b}) \\
 & + ([\mathbf{0}_{5N,3N} \quad \mathbf{I}_{5N}] \mathbf{y} - \tilde{\mathbf{q}})^\top ([\mathbf{0}_{5N,3N} \quad \mathbf{I}_{5N}] \mathbf{y} - \tilde{\mathbf{q}}) \\
 = & \mathbf{y}^\top \mathbf{A}^\top \mathbf{A} \mathbf{y} - 2\mathbf{y}^\top \mathbf{A}^\top \mathbf{b} + \mathbf{b}^\top \mathbf{b} \\
 & + \mathbf{y}^\top \begin{bmatrix} \mathbf{0}_{3N,3N} & \mathbf{0}_{3N,5N} \\ \mathbf{0}_{5N,3N} & \mathbf{I}_{5N} \end{bmatrix} \mathbf{y} - 2\mathbf{y}^\top \begin{bmatrix} \mathbf{0}_{3N,5N} \\ \mathbf{I}_{5N} \end{bmatrix} \tilde{\mathbf{q}} + \tilde{\mathbf{q}}^\top \tilde{\mathbf{q}}.
 \end{aligned} \tag{41}$$

The objective (24) can now be rewritten in terms of  $\mathbf{y}$  as

$$\begin{aligned}
 & \begin{bmatrix} \mathbf{c} \\ \mathbf{0}_{5N} \end{bmatrix} \mathbf{y} + \frac{\gamma}{2} \mathbf{y}^\top \left( \mathbf{A}^\top \mathbf{A} + \begin{bmatrix} \mathbf{0}_{3N,3N} & \mathbf{0}_{3N,5N} \\ \mathbf{0}_{5N,3N} & \mathbf{I}_{5N} \end{bmatrix} \right) \mathbf{y} \\
 & + \mathbf{y}^\top \left( \mathbf{A}^\top \boldsymbol{\mu}_1 + \begin{bmatrix} \mathbf{0}_{3N,5N} \\ \mathbf{I}_{5N} \end{bmatrix} \boldsymbol{\mu}_2 + \gamma \mathbf{A}^\top \mathbf{b} - \gamma \begin{bmatrix} \mathbf{0}_{3N,5N} \\ \mathbf{I}_{5N} \end{bmatrix} \tilde{\mathbf{q}} \right) \\
 & - \boldsymbol{\mu}_1^\top \mathbf{b} - \boldsymbol{\mu}_2^\top \tilde{\mathbf{q}} + \frac{\gamma}{2} \mathbf{b}^\top \mathbf{b} + \frac{\gamma}{2} \tilde{\mathbf{q}}^\top \tilde{\mathbf{q}}.
 \end{aligned} \tag{42}$$

We take the derivative w.r.t.  $\mathbf{y}$ :

$$\begin{aligned}
 & \begin{bmatrix} \mathbf{c} \\ \mathbf{0}_{5N} \end{bmatrix} + \gamma \left( \mathbf{A}^\top \mathbf{A} + \begin{bmatrix} \mathbf{0}_{3N,3N} & \mathbf{0}_{3N,5N} \\ \mathbf{0}_{5N,3N} & \mathbf{I}_{5N} \end{bmatrix} \right) \mathbf{y} + \mathbf{A}^\top \boldsymbol{\mu}_1 \\
 & + \begin{bmatrix} \mathbf{0}_{3N,5N} \\ \mathbf{I}_{5N} \end{bmatrix} \boldsymbol{\mu}_2 + \gamma \mathbf{A}^\top \mathbf{b} - \gamma \begin{bmatrix} \mathbf{0}_{3N,5N} \\ \mathbf{I}_{5N} \end{bmatrix} \tilde{\mathbf{q}} = \mathbf{0} \\
 & \gamma \left( \mathbf{A}^\top \mathbf{A} + \begin{bmatrix} \mathbf{0}_{3N,3N} & \mathbf{0}_{3N,5N} \\ \mathbf{0}_{5N,3N} & \mathbf{I}_{5N} \end{bmatrix} \right) \mathbf{y} \\
 = & - \begin{bmatrix} \mathbf{c} \\ \mathbf{0}_{5N} \end{bmatrix} - \mathbf{A}^\top \boldsymbol{\mu}_1 - \begin{bmatrix} \mathbf{0}_{3N} \\ \boldsymbol{\mu}_2 \end{bmatrix} - \gamma \mathbf{A}^\top \mathbf{b} + \gamma \begin{bmatrix} \mathbf{0}_{3N} \\ \tilde{\mathbf{q}} \end{bmatrix}
 \end{aligned} \tag{43}$$

which is the same as the linear system (25).

### B. Derivation of Thresholding Operation

We derive the solution to optimization (26). Ignoring the first convex but non-smooth term  $g(\tilde{\mathbf{q}})$ , the remaining two terms in the objective are convex and smooth. Taking the derivative w.r.t. variable  $\tilde{\mathbf{q}}$  and setting it to  $\mathbf{0}$ ,

$$\begin{aligned}
 -\boldsymbol{\mu}_2 - \gamma \mathbf{q}^{t+1} + \gamma \tilde{\mathbf{q}}^* &= \mathbf{0}_{5N} \\
 \tilde{\mathbf{q}}^* &= \mathbf{q}^{t+1} + \frac{1}{\gamma} \boldsymbol{\mu}_2.
 \end{aligned} \tag{44}$$

This solution is valid iff  $g(\tilde{\mathbf{q}}^*) = 0$ ; otherwise the first term  $g(\tilde{\mathbf{q}}^*)$  dominates and  $\tilde{\mathbf{q}}^* = \mathbf{0}_{5N}$ . Given that (44) can be computed entry-by-entry separately, (27) follows.

## APPENDIX

### A. Derivation of Linear System

We derive linear system (25) from optimization (24). For convenience, we first define  $\mathbf{y} = [\mathbf{x}; \mathbf{q}] \in \mathbb{R}^{8N}$ . Thus,

$$\begin{aligned}
 \mathbf{B} \begin{bmatrix} \mathbf{x} \\ \mathbf{q} \\ \tilde{\mathbf{q}} \end{bmatrix} &= \begin{bmatrix} \mathbf{b} \\ \mathbf{0}_{5N} \end{bmatrix} \\
 &= \begin{bmatrix} \mathbf{A} & \mathbf{0}_{6N,5N} \\ \mathbf{0}_{5N,3N} & \mathbf{I}_{5N} & -\mathbf{I}_{5N} \end{bmatrix} \begin{bmatrix} \mathbf{y} \\ \tilde{\mathbf{q}} \end{bmatrix} - \begin{bmatrix} \mathbf{b} \\ \mathbf{0}_{5N} \end{bmatrix} \\
 &= \begin{bmatrix} \mathbf{A}\mathbf{y} - \mathbf{b} \\ [\mathbf{0}_{5N,3N} \quad \mathbf{I}_{5N}] \mathbf{y} - \tilde{\mathbf{q}} \end{bmatrix}.
 \end{aligned} \tag{39}$$

Thus, the Lagrangian term becomes

$$\begin{aligned}
 & [\boldsymbol{\mu}_1^\top \quad \boldsymbol{\mu}_2^\top] \begin{bmatrix} \mathbf{A}\mathbf{y} - \mathbf{b} \\ [\mathbf{0}_{5N,3N} \quad \mathbf{I}_{5N}] \mathbf{y} - \tilde{\mathbf{q}} \end{bmatrix} \\
 &= \boldsymbol{\mu}_1^\top \mathbf{A} \mathbf{y} - \boldsymbol{\mu}_1^\top \mathbf{b} + \boldsymbol{\mu}_2^\top [\mathbf{0}_{5N,3N} \quad \mathbf{I}_{5N}] \mathbf{y} - \boldsymbol{\mu}_2^\top \tilde{\mathbf{q}} \\
 &= (\boldsymbol{\mu}_1^\top \mathbf{A} + \boldsymbol{\mu}_2^\top [\mathbf{0}_{5N,3N} \quad \mathbf{I}_{5N}]) \mathbf{y} - \boldsymbol{\mu}_1^\top \mathbf{b} - \boldsymbol{\mu}_2^\top \tilde{\mathbf{q}}
 \end{aligned} \tag{40}$$

where  $\boldsymbol{\mu}_1 \in \mathbb{R}^{6N}$  and  $\boldsymbol{\mu}_2 \in \mathbb{R}^{5N}$  are multiplier sub-vectors corresponding to variables  $\mathbf{y}$  and  $\tilde{\mathbf{q}}$ , respectively. Similarly, the